Article

Developmental Cell

YAP/TAZ Orchestrate VEGF Signaling during Developmental Angiogenesis

Graphical Abstract

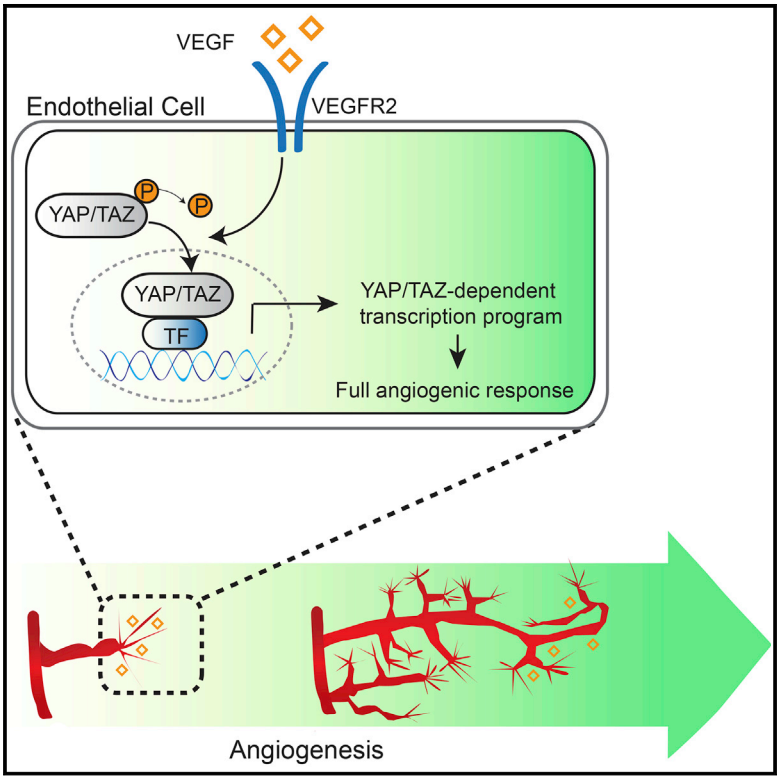

Highlights

- YAP/TAZ activity is controlled by VEGF during angiogenesis
- Endothelial expression of YAP/TAZ is essential for vascular system formation
- VEGF induces a YAP/TAZ-dependent transcriptome linked to cytoskeleton remodeling
- YAP/TAZ deletion results in impaired VEGFR2 cellular distribution and trafficking

Authors

Xiaohong Wang, Aida Freire Valls, Géza Schermann, ..., Tamás Fischer, Georg Halder, Carmen Ruiz de Almodóvar

Correspondence

carmen.ruizdealmodovar@bzh.uni-heidelberg.de

In Brief

Wang et al. identify YAP/TAZ as essential co-transcription factors in endothelial cells during developmental angiogenesis. They describe that YAP/TAZ are activated by VEGF and that their activity is needed for transducing the VEGF signal into a specific transcriptional program, required for a full angiogenic response.

Wang et al., 2017, Developmental Cell *42*, 462–478
September 11, 2017
http://dx.doi.org/10.1016/j.devcel.2017.08.002

CellPress

CellPress

Developmental Cell
Article

YAP/TAZ Orchestrate VEGF Signaling during Developmental Angiogenesis

Xiaohong Wang,[1] Aida Freire Valls,[1,2] Géza Schermann,[1] Ying Shen,[2] Ivan M. Moya,[3] Laura Castro,[1] Severino Urban,[1] Gergely M. Solecki,[4] Frank Winkler,[4] Lars Riedemann,[5] Rakesh K. Jain,[5] Massimilano Mazzone,[6,7] Thomas Schmidt,[2] Tamás Fischer,[1,8] Georg Halder,[3] and Carmen Ruiz de Almodóvar[1,9,*]

[1]Biochemistry Center (BZH), University of Heidelberg, Im Neuenheimer Feld 328, 69120 Heidelberg, Germany
[2]Department of General, Visceral and Transplantation Surgery, University Hospital Heidelberg, 69120 Heidelberg, Germany
[3]VIB-KU Leuven Center for Cancer Biology, Department of Oncology, KU Leuven, 3000 Leuven, Belgium
[4]Neurology Clinic and National Center for Tumor Diseases, University Hospital Heidelberg, 69120 Heidelberg, Germany
[5]Edwin L. Steele Laboratories, Department of Radiation Oncology, Massachusetts General Hospital and Harvard Medical School, Boston, MA 02114, USA
[6]Laboratory of Tumor Inflammation and Angiogenesis, Center for Cancer Biology, VIB, Leuven B3000, Belgium
[7]Laboratory of Tumor Inflammation and Angiogenesis, Center for Cancer Biology, Department of Oncology, KU Leuven, 3000 Leuven, Belgium
[8]Genome Biology Department, The John Curtin School of Medical Research, The Australian National University, Garran Road, Canberra, ACT 2601, Australia
[9]Lead Contact
*Correspondence: carmen.ruizdealmodovar@bzh.uni-heidelberg.de
http://dx.doi.org/10.1016/j.devcel.2017.08.002

SUMMARY

Vascular endothelial growth factor (VEGF) is a major driver of blood vessel formation. However, the signal transduction pathways culminating in the biological consequences of VEGF signaling are only partially understood. Here, we show that the Hippo pathway effectors YAP and TAZ work as crucial signal transducers to mediate VEGF-VEGFR2 signaling during angiogenesis. We demonstrate that YAP/TAZ are essential for vascular development as endothelium-specific deletion of YAP/TAZ leads to impaired vascularization and embryonic lethality. Mechanistically, we show that VEGF activates YAP/TAZ via its effects on actin cytoskeleton and that activated YAP/TAZ induce a transcriptional program to further control cytoskeleton dynamics and thus establish a feedforward loop that ensures a proper angiogenic response. Lack of YAP/TAZ also results in altered cellular distribution of VEGFR2 due to trafficking defects from the Golgi apparatus to the plasma membrane. Altogether, our study identifies YAP/TAZ as central mediators of VEGF signaling and therefore as important regulators of angiogenesis.

INTRODUCTION

Proper organ vascularization requires that the vascular system grows and integrates itself within all other cellular types of the specific organ. For this to occur the vasculature needs to be instructed when, how, and how much it should grow. Deregulation of these processes is a hallmark of many diseases, including developmental disorders, cancer, and cardiovascular diseases.

The study of the functional effects on blood vessels induced by one of the main angiogenic factors, vascular endothelial growth factor (VEGF), is an intense research subject (Chung and Ferrara, 2011). During a vascularization process VEGF regulates numerous processes, including endothelial cell (EC) proliferation, migration, and cell survival (Chung and Ferrara, 2011). While intracellular signaling pathways upon VEGF stimulation have been extensively studied, it remains unclear how the VEGF signal is transmitted into transcriptional programs and the specific consequences of these programs.

YAP and TAZ, two related transcriptional co-activators, have been identified as master regulators of organ growth (Halder and Johnson, 2011; Piccolo et al., 2014). Their activity is mainly regulated by the Hippo pathway. The core components of this pathway comprise a kinase cascade containing Mst1/2 and Lats1/2. Mst1/2 phosphorylates and activates Lats1/2, which then phosphorylate YAP/TAZ, causing their cytoplasmic sequestration, degradation, and inactivation (Halder and Johnson, 2011; Piccolo et al., 2014). When activated, YAP/TAZ shuffle from the cytosol to the nucleus where they interact with different transcription factors (of which TEAD transcription factors are the best characterized) to regulate expression of a large group of target genes primarily involved in cell growth, survival, and migration (Zanconato et al., 2016).

Recent studies show that the Hippo/YAP/TAZ pathway can be regulated by diverse stimuli such as mechanical cues, cell polarity, biochemical factors, cellular energy stress, growth factors, G-protein-coupled receptors (GPCRs), and Wnts (Yu et al., 2012; Zanconato et al., 2016). Despite these findings, there are still open questions regarding how their activity is regulated *in vivo* and whether this is organ dependent. In this respect, it remains unknown how YAP/TAZ activity is controlled in the vascular system during angiogenesis, what are the molecular determinants triggering it, and what are the functional consequences of YAP/TAZ inactivation.

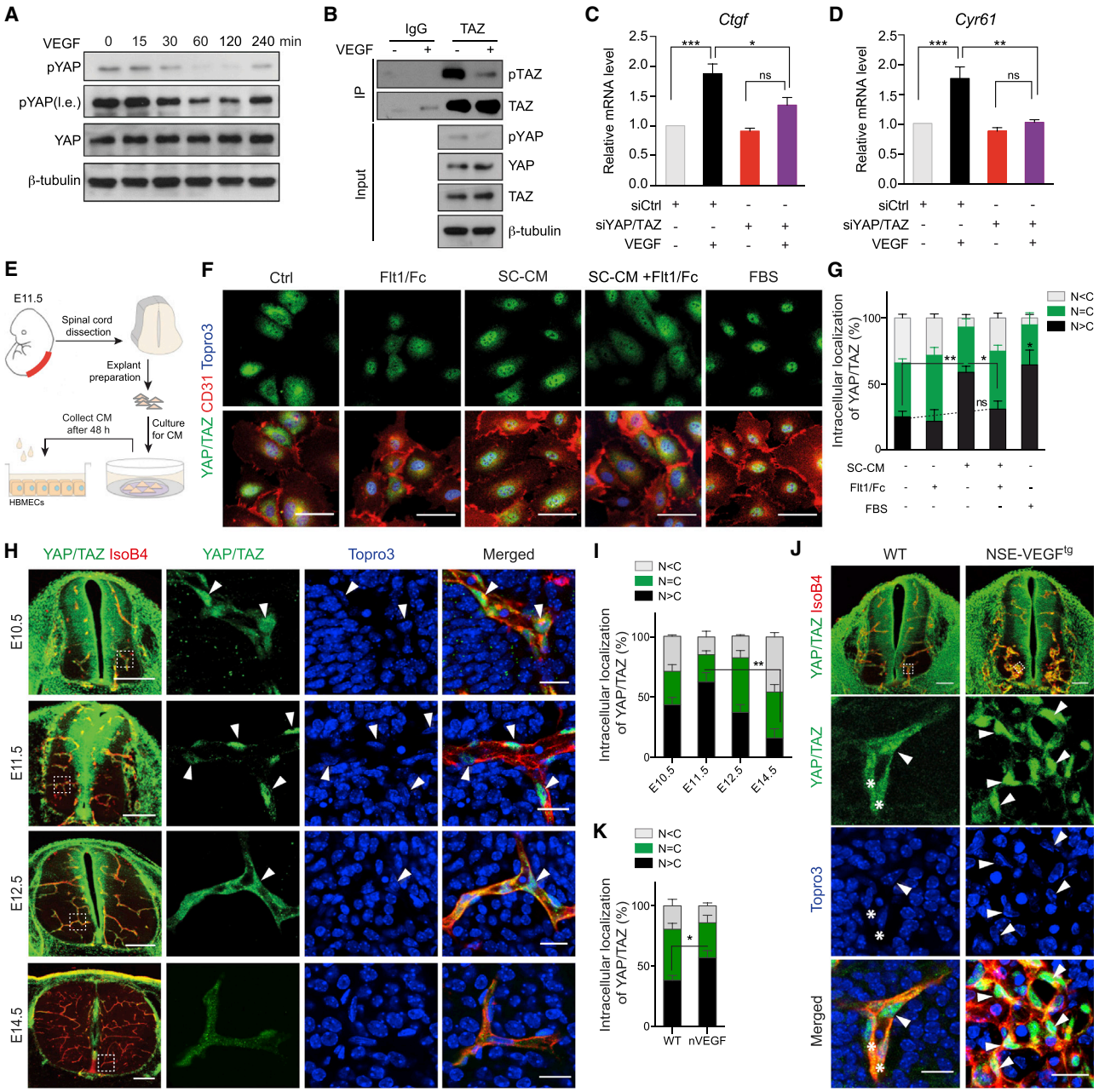

Figure 1. VEGF Regulates YAP/TAZ Activity

(A) Western blot detection of YAP phosphorylation status in subconfluent MBEs stimulated with VEGF for the indicated time points. l.e., long film exposure.

(B) Immunoprecipitation (IP) of TAZ followed by immunoblot for pTAZ in MBEs treated with VEGF for 2 hr showing reduced phosphorylation of TAZ upon VEGF. Blots for pYAP, YAP, and TAZ are also shown in the input. IgG, immunoglobulin G.

(C and D) Relative mRNA level of *Ctgf* (C) and *Cyr61* (D) in MBEs transfected with control (Ctrl) siRNA or YAP/TAZ siRNA and treated with VEGF for 6 hr; data are normalized to control conditions, n = 4 independent experiments.

(E) Workflow for the generation of SC-CM and subsequent stimulation of HBMECs.

(F) Representative images of HBMECs exposed to SC-CM, in the presence or absence of sFlt1/Fc for 2 hr. Immunofluorescence for YAP/TAZ, CD31 (EC marker), and nuclei (Topro3) is shown. Scale bars, 50 μm.

(G) Quantification of YAP/TAZ cellular localization for HBMECs treated as in (F). Data from approximately 200 cells from 12 random fields of view (at least 3 independent experiments). N, nucleus; C, cytosol.

(H) Representative images of mouse embryos at different developmental stages immunostained for YAP/TAZ, ECs (IsoB4), and nuclei (Topro3). Images are representative of 3 litters per developmental stage. Scale bars, 200 μm (lower magnification) and 20 μm (insets).

(I) Quantification of YAP/TAZ cellular localization for the different embryonic stages shown in (H) (n = 3 [E10.5], 5 [E11.5], 4 [E12.5], and 4 [E14.5]). N, nucleus; C, cytosol.

(legend continued on next page)

Depletion of a single VEGF allele in mice results in embryonic lethality due to severe vascular malformations in the embryo and the yolk sac (Carmeliet et al., 1996). Similarly, YAP depletion results in developmental embryonic arrest with the highlight of vascular defects in the yolk sac (Morin-Kensicki et al., 2006). Notably, the YAP/TAZ target genes connective tissue growth factor (*CTGF*) and cysteine-rich 61 (*CYR61*) are upregulated upon VEGF stimulation and serve as mediators of the VEGF-triggered angiogenic response (Brigstock, 2002; Morin-Kensicki et al., 2006). Recently, YAP was described to be expressed in ECs of the developing mouse retina, showing an enriched expression and nuclear localization in the angiogenic front (Choi et al., 2015). Interestingly, this pattern of YAP activation nicely fits with the described gradient of VEGF receptor (VEGFR) signaling in the retinal developing vasculature (Nakayama et al., 2013). Prompted by these observations, we wondered whether there is a potential connection between the Hippo and the VEGF signaling pathways during vascular development.

Here, we identify YAP/TAZ as critical transducers of VEGF signaling in ECs. We show that YAP/TAZ are essential for the formation of the vascular system. Once activated by VEGF, YAP/TAZ act as co-transcription factors and induce a transcriptional program resulting in expression of genes involved in cytoskeleton organization, cell migration, and protein trafficking. In the absence of YAP/TAZ, cytoskeleton rearrangements and VEGFR2 trafficking from the Golgi to the plasma membrane are impaired, resulting in altered VEGFR2 cellular distribution and signaling, reduced cell migration, and compromised angiogenesis. Taken together, our study reveals a new role for YAP/TAZ in regulating VEGF signaling and provides new insights into how VEGF signaling is translated into biological effects to control angiogenesis.

RESULTS

VEGF Triggers YAP/TAZ Activation

To investigate whether there is any crosstalk between the Hippo/YAP/TAZ pathway and VEGF signaling, we first determined whether VEGF regulates YAP/TAZ activity. As we observed that the ratio between TAZ and YAP expression in different ECs is much higher than in other non-EC cell types (Figures S1A and S1B), we checked the phosphorylation status of both YAP and TAZ upon VEGF stimulation. VEGF treatment resulted in a hypo-phosphorylation of YAP in several ECs, including mouse brain endothelioma cells (MBEs) (Figure 1A), human brain microvascular ECs (HBMECs), and human umbilical vein ECs (HUVECs) (Figure S1C). Similarly, reduced phospho-TAZ was also detected after VEGF stimulation (Figure 1B). The VEGF activation of YAP/TAZ was further demonstrated by increased YAP/TAZ nuclear translocation in HBMECs (Figures S1D and S1E), and in isolated primary mouse brain ECs (Figures S1F and S1G). As the LPA and S1P lipids present in serum can activate YAP/TAZ (Yu et al., 2012), we used fetal bovine serum (FBS) as a positive control of YAP/TAZ activation (Figures 1F, 1G, S1D–S1G, and S1L–S1N). Analysis of mRNA levels of *CTGF* and *CYR61* revealed a significant increase in MBEs and HBMECs upon VEGF treatment (Figures 1C, 1D, S1H, and S1I). This effect was indeed YAP/TAZ dependent, as VEGF had no effect in YAP/TAZ knockdown MBEs using small interfering RNAs for YAP and TAZ (siYAP/TAZ) (Figures 1C, 1D, and S1J).

Upon nuclear translocation, YAP/TAZ bind to TEAD transcription factors to induce transcription of specific target genes. We further confirmed that VEGF induces YAP/TAZ activity by analyzing transcriptional activation of TEAD-responsive elements (Zhao et al., 2008). For this, we co-transfected HEK293 cells with a plasmid encoding for VEGFR2 and a synthetic luciferase sensor containing multimerized responsive elements of TEAD, 8xGTIIC-Lux (Dupont et al., 2011). VEGF stimulation triggered induction of luciferase expression (Figure S1K), indicating that VEGF is able to activate YAP/TAZ.

During embryonic mouse spinal cord (SC) development, VEGF is expressed in the neuroepithelium and plays a key role in regulating its vascularization (Himmels et al., 2017). We thus explored whether SC-derived VEGF also regulates YAP/TAZ. First, we microdissected SCs from embryonic day 11.5 (E11.5) embryos, made explants, and generated conditioned medium (SC-CM), with which we treated HBMECs in culture (Figure 1E). Stimulation of HBMECs with SC-CM resulted in VEGFR2 activation, indicating that VEGF is secreted by these explants (Figure S1L). SC-CM also caused a significant nuclear accumulation of YAP/TAZ in HBMECs (Figures 1F and 1G) and a significant increase in mRNA levels of *CTGF* and *CYR61* (Figures S1M and S1N). VEGF present in the SC-CM was the activating cue as the addition of recombinant soluble Flt1/Fc (which traps VEGF) blocked YAP/TAZ activation (Figures 1F, 1G, and S1L–S1N).

Based on these results, we examined YAP/TAZ activation status *in vivo* at different developmental stages where VEGF is expressed in the SC (Himmels et al., 2017). Interestingly, YAP/TAZ subcellular localization showed a dynamic pattern in ECs. While at early developmental stages (E10.5 and E11.5) YAP/TAZ are prominently enriched in the nucleus, suggesting that they are active, in later developmental stages (E14.5) the majority of ECs have YAP/TAZ in the cytosol (Figures 1H and 1I).

To further validate that neuronal derived VEGF regulates YAP/TAZ activity *in vivo*, we made use of the transgenic mouse line NSE-VEGF^{tg}, which overexpresses the human VEGF$_{165}$ isoform in neurons (Wang et al., 2005) and has increased vascular density in the embryonic SC (Himmels et al., 2017) (Figure 1J). In NSE-VEGF^{tg} embryos, nuclear YAP/TAZ in ECs was aberrantly elevated compared with control embryos, indicating that increased VEGF signaling is sufficient to induce an enrichment of YAP/TAZ in the nucleus of ECs *in vivo* (Figures 1J and 1K).

(J) Representative confocal images of E10.5 NSE-VEGF^{tg} and wild-type (WT) littermate embryos stained for YAP/TAZ, ECs (IsoB4), and nuclei (Topro3). Images are representative of embryos of 3 litters. Note that in NSE-VEGF^{tg} embryos YAP/TAZ are enriched in the nucleus of ECs. Scale bars, 100 μm (lower magnification) and 20 μm (insets).

(K) Quantification of YAP/TAZ cellular localization in WT and NSE-VEGF^{tg} embryos showing enriched nuclear YAP/TAZ in NSE-VEGF^{tg} (n = 7 [WT] and 8 [NSE-VEGF^{tg}]). N, nucleus; C, cytosol.

In (H) and (J), white arrowheads point to nuclear YAP/TAZ in ECs. Asterisks in (J) show cytosolic YAP/TAZ. For (C), (D), (G), (I), and (K), data represent mean ± SEM (*$p < 0.05$, **$p < 0.01$, ***$p < 0.001$; ns, not significant). See also Figure S1.

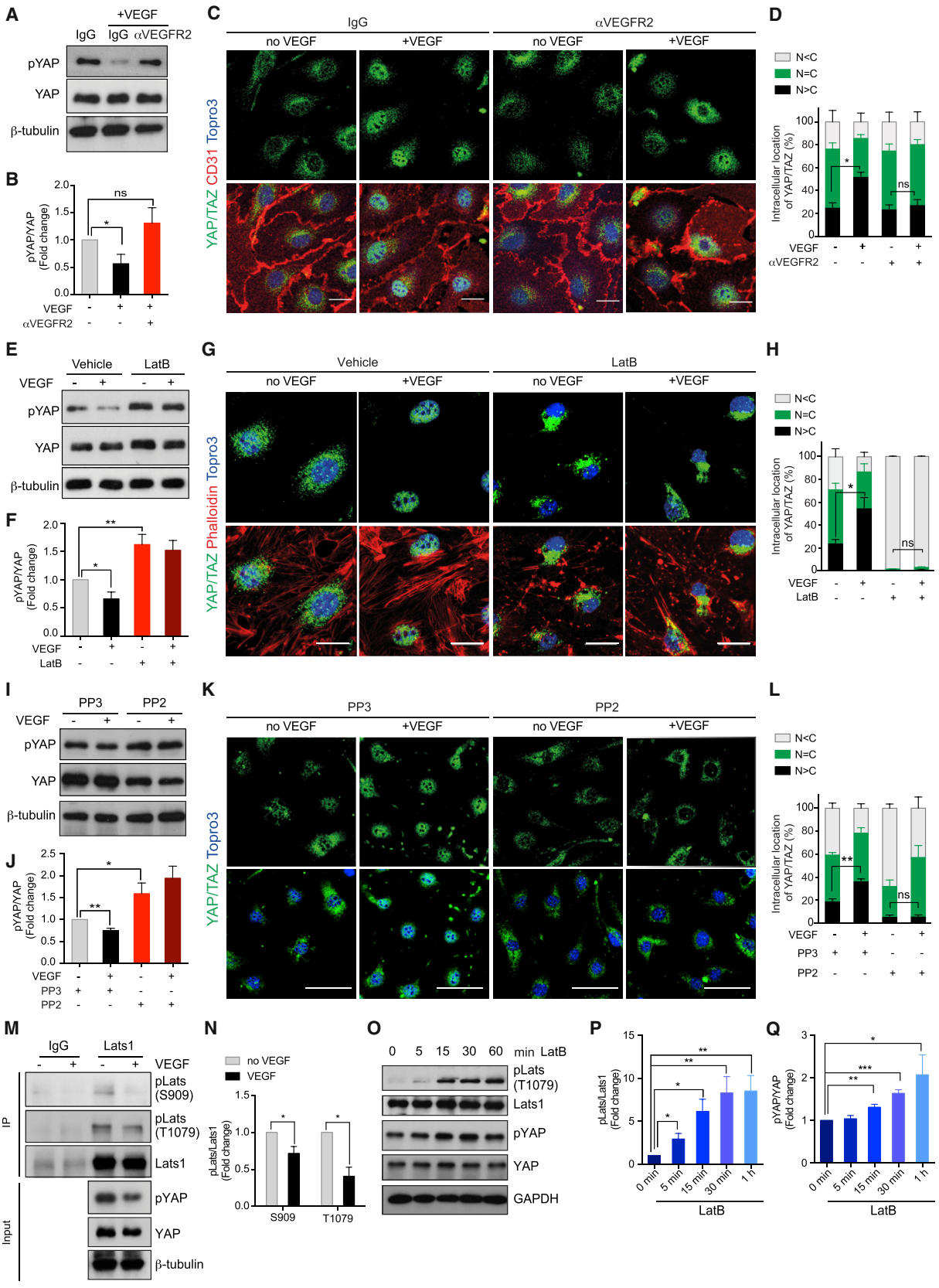

(legend on next page)

YAP/TAZ Localize to the Nucleus of ECs during Pathological Angiogenesis

To determine whether YAP/TAZ nuclear localization in ECs also occurs during pathological angiogenesis, we used the U87 glioblastoma tumor model (Figure S1O), known to be highly vascularized due to high VEGF expression (Wachsberger et al., 2007). We analyzed brain sections of tumor-bearing mice 34 days after ipsilateral injection of U87 tumor cells into the cortex. While in ECs from normal cortical vessels YAP/TAZ were exclusively localized in the cytosol, in tumor-associated ECs YAP/TAZ were highly accumulated in the nucleus (Figure S1P). This result indicates that in an active process of pathological angiogenesis YAP/TAZ are also activated in ECs.

VEGF-Mediated Actin Cytoskeleton Changes Are Crucial for YAP/TAZ Activation

Next, we aimed to understand how VEGF triggers YAP/TAZ activation. As reduced YAP and TAZ phosphorylation occurred in a similar manner (Figures 1A and 1B), we continued our analysis by monitoring only YAP phosphorylation status. To confirm that VEGF acts via VEGFR2 signaling to control YAP/TAZ activity, we stimulated MBEs in the presence of a VEGFR2 functional blocking antibody (αVEGFR2). VEGFR2 blockage inhibited VEGF-induced phospho-YAP reduction (Figures 2A and 2B), YAP/TAZ nuclear accumulation (Figures 2C and 2D), and increase in *Ctgf* and *Cyr61* mRNA (Figures S2A and S2B).

Recent studies showed that mechanical cues such as extracellular matrix (ECM) stiffness, cell geometry, and cytoskeletal dynamics serve as regulators of YAP/TAZ activity (Halder et al., 2012; Yu et al., 2012). VEGF is known to regulate cytoskeleton dynamics and similarly promote EC migration (Lamalice et al., 2007). Therefore, we wondered whether VEGF-induced changes in actin dynamics are mediators of VEGF-induced activation of YAP/TAZ. We used an actin-disrupting agent, Latrunculin B (LatB), to prevent actin polymerization, as previously done (Yu et al., 2012). In the presence of LatB, VEGF stimulation did not result in reduced phospho-YAP (Figures 2E and 2F), YAP/TAZ nuclear translocation (Figures 2G and 2H), or induction of YAP/TAZ target gene expression (Figures S2C and S2D). LatB treatment did not interfere with VEGFR2 activation (Figure S2E). These results suggest that an intact actin cytoskeleton is necessary for VEGF-mediated regulation of YAP/TAZ activity.

To elucidate further the mechanism of how VEGF regulates cytoskeleton actin dynamics to control YAP/TAZ activation, we focused on Src family kinases (SFKs) and Rho guanosine triphosphatases (GTPases), as both have been implicated in VEGF-mediated cytoskeleton changes. SFKs are known as VEGFR2 downstream signaling modulators that, via reorganizing the cytoskeleton, control VEGF-mediated EC migration and vascular permeability (Sun et al., 2012). In this context, we explored whether SFKs participate in the VEGF-YAP/TAZ axis. Blocking SFKs with the widely used inhibitor PP2, but not with its inactive analog PP3 (Figure S2F), attenuated VEGF-induced reduction in YAP phosphorylation (Figures 2I and 2J), the induction of YAP/TAZ nuclear accumulation (Figures 2K and 2L), and the induction of *Ctgf* and *Cyr61* mRNA expression (Figures S2G and S2H).

The Rho family of GTPases is important for mediation of VEGF-induced cytoskeleton changes in ECs (van Nieuw Amerongen et al., 2003). In addition, Rho GTPases are regarded as YAP/TAZ regulators in different cell types (Dupont et al., 2011; Ohgushi et al., 2015; Yu et al., 2012). Therefore, we used a specific inhibitor of Rho GTPases, *botulinum* toxin C3 transferase, and tested the effect of VEGF on YAP/TAZ activation. In cells pretreated with C3 transferase (as previously done (Yu et al., 2012)), VEGF was no longer able to efficiently induce YAP/TAZ nuclear translocation, nor to increase *Ctgf* and *Cyr61* mRNA levels (Figures S2I–S2K).

Thus, consistent with previous studies reporting that actin cytoskeleton dynamics lead to YAP activation (Dupont et al., 2011; Wada et al., 2011; Zhao et al., 2012), our results also support a model whereby VEGF-induced actin cytoskeleton changes result in YAP/TAZ activation in ECs. In particular,

Figure 2. VEGF-VEGFR2 Signaling Regulates YAP/TAZ Activity in a Cytoskeleton-Dependent Manner

(A) Western blot showing pYAP status in MBEs pretreated with 5 μg/mL control IgG or αVEGFR2 for 2 hr and then stimulated with VEGF for another 2 hr.

(B) Quantification of western blot shown in (A); n = 3 independent experiments.

(C) Immunofluorescence for YAP/TAZ, CD31 and nuclei (Topro3) in MBEs treated as in (A). Scale bars, 20 μm.

(D) Quantification of YAP/TAZ subcellular localization in MBEs shown in (C). Note that VEGF induces YAP/TAZ nuclear translocation and that αVEGFR2 abolishes this effect. N, nucleus; C, cytosol.

(E) Western blot showing pYAP status in MBEs pretreated with 1 μg/mL LatB for 30 min and stimulated with VEGF for 2 hr.

(F) Quantification of western blot shown in (E); n = 4 independent experiments.

(G) Immunofluorescence images showing YAP/TAZ subcellular localization and actin cytoskeleton (phalloidin) in MBEs treated as in (E) showing that blocking actin polymerization blocks VEGF-induced YAP/TAZ nuclear translocation. Scale bars, 20 μm.

(H) Quantification of subcellular localization of YAP/TAZ shown in (G). N, nucleus; C, cytosol.

(I) Western blot showing pYAP status in MBEs pretreated with 10 μM PP3 or PP2 for 1 hr and stimulated with VEGF for 2 hr.

(J) Quantification of western blot shown in (I); n = 4 independent experiments.

(K) YAP/TAZ subcellular localization in MBEs treated as in (I) is shown by immunofluorescence. Note that blocking SFKs impairs VEGF-mediated YAP/TAZ activation. Scale bars, 50 μm.

(L) Quantification of subcellular localization of YAP/TAZ shown in (H). N, nucleus; C, cytosol.

(M) Immunoprecipitation (IP) of endogenous Lats1 from MBEs stimulated with VEGF for 2 hr, followed by immunoblot for pLats (S909 or T1079), showing reduced phosphorylation of Lats1 upon VEGF stimulation.

(N) Quantification of western blot shown in (M); n = 4 independent experiments.

(O) Immunoblot for pLats (T1079) and pYAP in HBMECs treated with 1 μg/mL of LatB showing a time-dependent increase of Lats1 and YAP phosphorylation.

(P and Q) Quantification of western blot shown in (O); n = 3 independent experiments.

For (D), (H), and (L), cells from 12 random fields of view from 3 independent experiments (≈200 cells) were quantified. For (B), (D), (F), (H), (J), (L), (N), (P), and (Q), data are expressed as mean ± SEM (*p < 0.05, **p < 0.01, ***p < 0.001; ns, not significant). See also Figure S2.

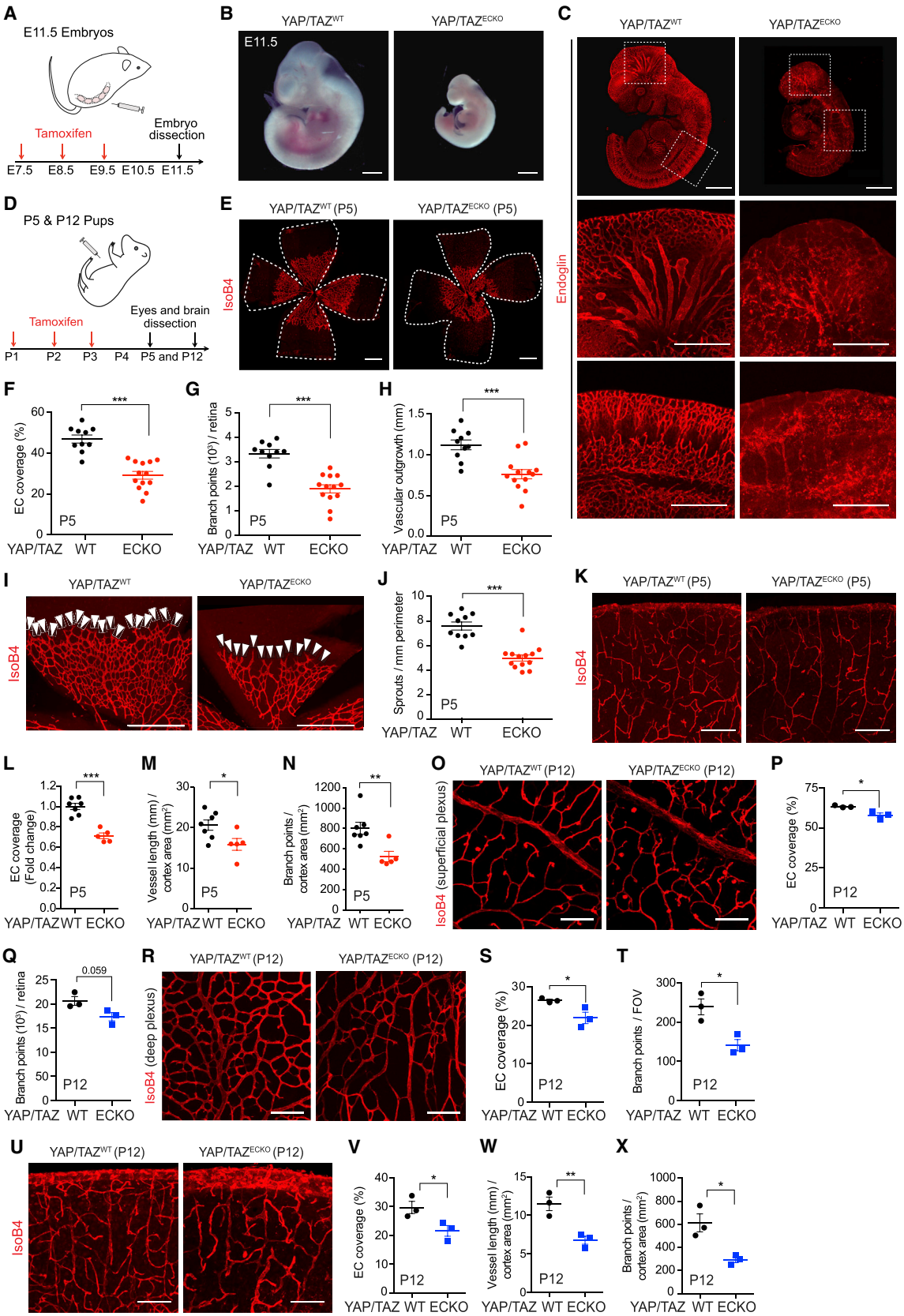

(legend on next page)

VEGF requires SFKs and Rho GTPases to activate YAP/TAZ, presumably via regulating actin dynamics.

Modulation of YAP/TAZ activity via the cytoskeleton could occur with or without affecting the activity of Lats1/2 (Dupont et al., 2011; Yu et al., 2012). We therefore tested the effect of VEGF on Lats1 phosphorylation. VEGF stimulation decreased Lats1 phosphorylation at the two sites that determine its activity (Figures 2M and 2N), indicating that Lats1 activity is reduced by VEGF. Moreover, we observed that LatB leads to phosphorylation of Lats1, and consistently also to an increase in phospho-YAP (Figures 2O–2Q). Altogether, these results indicate that the regulation of Lats1 activity in ECs requires a functional actin cytoskeleton and suggest that Lats1 contributes to VEGF-mediated activation of YAP/TAZ.

YAP/TAZ Endothelial Specific Knockout Results in Impaired Angiogenesis *In Vivo*

Prompted by the *in vitro* regulation of YAP/TAZ activity by VEGF, together with the observed dynamic subcellular localization of YAP/TAZ in ECs during developmental angiogenesis, we went on to elucidate the physiological significance of YAP/TAZ in ECs during development.

Besides expression in SC ECs, we observed a wide expression of YAP/TAZ in ECs of different developing organs, such as embryonic hindbrain, dorsal aorta, lung, and mouse limb (Figures S3A–S3C), and in postnatal brain and retina ECs (Figures S3D and S3E). Nuclear localization of YAP/TAZ in retina ECs was observed in the growing vascular front (Figure S3E), complementing previous studies where only YAP expression was shown (Choi et al., 2015). Interestingly, despite the fact that YAP/TAZ are localized in the nucleus of EC tip cells (Figure S3E), no proliferation is observed in tip cells (Gerhardt et al., 2003), suggesting that unknown mechanisms might be present in these cells to inhibit YAP/TAZ-mediated proliferation but to allow other YAP/TAZ-dependent effects.

As YAP and TAZ are functionally redundant during development (Nishioka et al., 2009) and in ECs their activation occurs similarly upon VEGF stimulation, we knocked out both together in ECs by crossing YAP/TAZ double-floxed mice (Xin et al., 2011, 2013) to the EC-specific *Cdh5-(PAC)-CreER*^{T2} mouse line (Wang et al., 2010) (Cdh5(PAC)$^{CreERT2/+}$;YAP$^{fl/fl}$;TAZ$^{fl/fl}$, hereafter termed YAP/TAZ^{ECKO}).

Inactivation of YAP/TAZ in ECs during embryonic development (Figure 3A) resulted in severe vascular defects throughout the whole body and yolk sac (Figures 3B, 3C, and S4A–S4C) and, as a consequence, in developmental arrest and embryonic lethality. Thus, highlighting the essential role of YAP/TAZ during vascular development. To study postnatal angiogenesis we mainly focused on retina and brain vascularization. Postnatal inactivation of YAP/TAZ in ECs (Figures 3D and S4D–S4G) also resulted in severe vascular defects. Quantification of postnatal day 5 (P5) whole-mount retinas showed a reduction of vascular area, blood vessel branching (Figures 3E–3G), and reduced radial outgrowth (Figure 3H) in YAP/TAZ^{ECKO} compared with YAP/TAZ^{WT} littermates. Quantification of sprouts at the vascular leading front also revealed a significant reduction in YAP/TAZ^{ECKO} retinas (Figures 3I and 3J). In addition, the number of proliferative ECs was reduced in YAP/TAZ^{ECKO} retinas (Figures S4H and S4I). No changes were observed in blood vessel regression (Figures S4J and S4K), suggesting that vessel remodeling was not affected in YAP/TAZ^{ECKO} retinas during development. In the developing brain cortex, YAP/TAZ^{ECKO} P5 pups showed a significant reduction in vessel coverage, vessel length, and branch points (Figures 3K–3N). Hemorrhages in YAP/TAZ^{ECKO} brains were also seen, indicating impaired vessel function and increased leakiness (Figure S4L).

We also analyzed developmental angiogenesis in the retinas and brains of P12 pups as well as in other organs (Figure 3D). While we did not observe any difference in organ weight at P5 (Figure S5A), analysis at P12 showed that YAP/TAZ^{ECKO} pups

Figure 3. EC-Specific Deletion of YAP/TAZ Results in Vascular Defects during Embryonic and Postnatal Development

(A) Scheme of tamoxifen injection in pregnant females.

(B) YAP/TAZ^{WT} and YAP/TAZ^{ECKO} mouse embryos at E11.5. Scale bars, 1 mm.

(C) Whole-mount immunostaining for the EC marker Endoglin, showing impaired vascular development in YAP/TAZ^{ECKO} embryos (E11.5). Upper panels: embryo overview (scale bars, 1 mm). Middle and lower panels: insets showing the vasculature in the brain and the intersomitic vessels (scale bars, 500 μm).

(D) Scheme of tamoxifen injection in YAP/TAZ^{WT} and YAP/TAZ^{ECKO} mouse pups.

(E) Whole-mount P5 retinas stained with IsoB4 (ECs). The white line highlights total retina area. Scale bars, 500 μm.

(F–H) Quantitative analysis at P5 shows reduced vascular coverage (F), branch points (G), and radial outgrowth (H) in YAP/TAZ^{ECKO} retinas compared with YAP/TAZ^{WT} (n = 10 WT, n = 13 KO).

(I) Representative confocal images of a P5 retina lobe stained with IsoB4 showing reduced number of sprouts (white arrowheads) at the vascular front of YAP/TAZ^{ECKO} retinas compared with YAP/TAZ^{WT}. Scale bars, 500 μm.

(J) Quantification of the number of sprouts shown in (I) showing reduced number in YAP/TAZ^{ECKO} mice compared with YAP/TAZ^{WT} (n = 10 WT, n = 13 KO).

(K) Representative confocal images of the brain cortical vasculature of P5 pups stained with IsoB4. Scale bars, 200 μm.

(L–N) Quantification of vascular coverage (L), total vessel length (M), and number of branch points (N) shows reduced vascularization in the cortex of YAP/TAZ^{ECKO} mice (n = 7 WT, n = 5 KO).

(O) Staining of P12 retinal superficial vascular plexus (IsoB4). Scale bars, 100 μm.

(P and Q) Quantitative analysis in the superficial retinal vascular plexus at P12 showing reduced vascular coverage (P) and a trend toward fewer branches (Q) in YAP/TAZ^{ECKO} mice compared with YAP/TAZ^{WT} (n = 3 WT, n = 3 KO).

(R) Staining of P12 retinal deep vascular plexus (IsoB4). Scale bars, 100 μm.

(S and T) Quantitative analysis of the deep vascular plexus showing a reduced vascular coverage (S) and branch points (per field of view [FOV]) (T) in YAP/TAZ^{ECKO} retinas compared with YAP/TAZ^{WT} (n = 3 WT, n = 3 KO).

(U) Representative confocal images of the brain cortical vasculature (IsoB4) of P12 pups. Scale bars, 100 μm.

(V–X) Quantification of vascular coverage (V), total vessel length (W), and number of branch points (X) shows reduced vascularization in the cortex of YAP/TAZ^{ECKO} pups (n = 3 WT, n = 3 KO).

For (F–H), (J), (L–N), (P), (Q), (S), (T), and (V–X), data represent mean ± SEM (*p < 0.05, **p < 0.01, ***p < 0.001). See also Figures S3–S5.

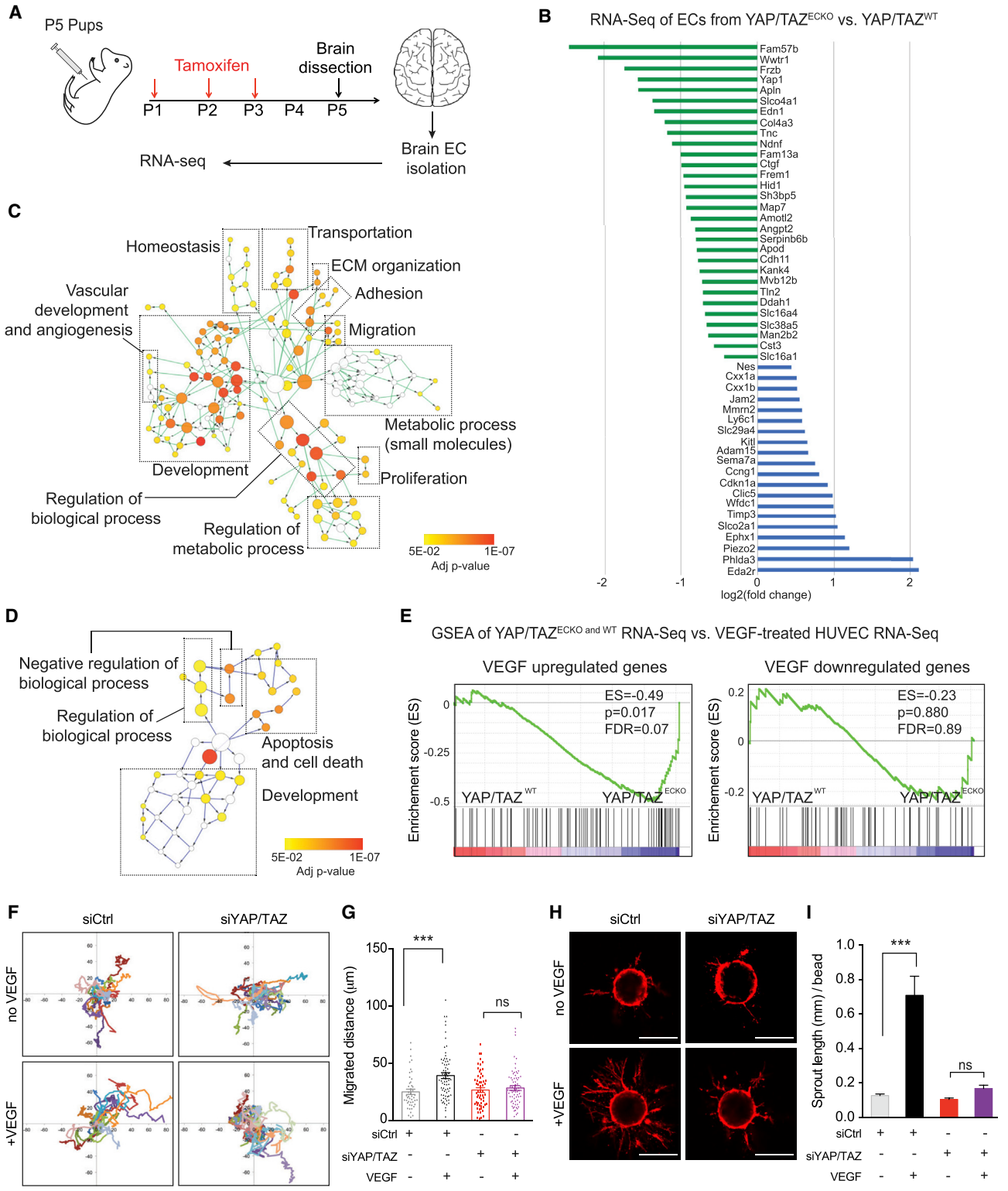

Figure 4. YAP/TAZ Knockout in Brain ECs Results in a Lack of Response to VEGF Stimulation

(A) Workflow for RNA-seq in isolated brain ECs from YAP/TAZ^{ECKO} and YAP/TAZ^{WT} pups.

(B) Top 50 significantly changed genes detected by RNA-seq in brain ECs of YAP/TAZ^{ECKO} compared with YAP/TAZ^{WT} (downregulated [green], upregulated [blue]).

(C and D) Network visualization of GO terms for downregulated (C) and upregulated genes (D) in YAP/TAZ^{ECKO} compared with YAP/TAZ^{WT} brain ECs.

(E) GSEA analysis of the VEGF-regulated genes (12 hr) in HUVECs over YAP/TAZ^{WT} and YAP/TAZ^{ECKO} brain ECs RNA-seq data.

(legend continued on next page)

weighed significantly less than YAP/TAZ^{WT} (Figure S5B) and that several organs were significantly lighter (Figure S5C). At P12 vascular defects of the retinas were most prominently observed in the deeper vascular plexus (Figures 3O–3T). Similar vascular defects as in P5 were observed in the brain of P12 YAP/TAZ^{ECKO} pups (Figures 3U–3X). Hemorrhages in P12 retinas and brains were also seen (Figures S5D and S5E). Interestingly, while blood vessel density in the liver of P5 pups was not affected (Figures S5F and S5G), a significant reduction in liver vascularization was observed at P12 (Figures S5H and S5I).

Taken together, our results indicate that YAP/TAZ in ECs serve as essential regulators of angiogenesis during embryonic and postnatal development. Postnatally, this essential role for YAP/TAZ is first manifested in the CNS but also becomes evident in other organs (i.e., liver) later after YAP/TAZ depletion (P12).

VEGF Induces a YAP/TAZ-Dependent Transcriptional Program to Regulate Angiogenesis

To investigate the underlying mechanism of the observed vascular phenotype, we performed transcriptome analysis of isolated brain ECs from YAP/TAZ^{WT} or YAP/TAZ^{ECKO} P5 pups (Figures 4A and S6A). We identified 256 significantly changed genes (137 downregulated and 119 upregulated genes) in YAP/TAZ^{ECKO} compared with YAP/TAZ^{WT} (absolute $\log_2$ fold change >0.5, $p_{adj} < 0.05$) (Figures 4B and S6B; Table S1). Gene Ontology (GO) analysis followed by network visualization of enriched GO terms using BiNGO (Figures 4C and 4D) showed that while the downregulated genes are linked to proliferation, adhesion, migration, regulation of metabolic processes, development, and angiogenesis (Figure 4C), the upregulated genes are mainly involved in apoptosis and cell death (Figure 4D). Consistent with published studies (Choi et al., 2015), angiopoietin-2 (Ang2) was downregulated in YAP/TAZ^{ECKO} ECs (Figure 4B).

We next determined whether the transcriptome changes due to YAP/TAZ deletion correlated with the ones caused by VEGF stimulation. For this, we performed gene set enrichment analysis (GSEA) using previously reported data for VEGF stimulation in ECs (Zhang et al., 2013) (Table S2). Importantly, genes that were upregulated upon VEGF stimulation were significantly enriched in the gene sets that were decreased by YAP/TAZ depletion (Figure 4E), indicating that YAP/TAZ are required for the induction of expression of those genes upon VEGF stimulation.

To explore the functional role of those overlapping genes, we performed KEGG signaling pathway analysis. Interestingly, these genes were mainly correlated to the phosphatidylinositol 3-kinase-Akt signaling pathway, ECM-receptor interaction, and focal adhesion and regulation of actin cytoskeleton (Figure S6C). As most of the prominent identified pathways are known to play a role in cell migration (Lamalice et al., 2007), these results suggest that the YAP/TAZ-induced transcriptional program might be important for regulating the migratory response of ECs upon VEGF.

YAP/TAZ Play a Crucial Role in VEGF-Regulated EC Migration and Angiogenesis

To determine whether YAP/TAZ are indeed needed for EC migration after VEGF stimulation, we silenced YAP/TAZ in MBEs and/or HBMECs (Figures S1J and S6D) and analyzed the migration and angiogenesis capacity of ECs *in vitro* performing a scratch assay. While VEGF induced the closure of the gap by 80% in control cells, this effect was abolished in YAP/TAZ knockdown cells (Figures S6E and S6F). Under non-stimulated conditions the knockdown of YAP/TAZ also resulted in reduced closure of the gap (Figures S6E and S6F).

YAP/TAZ^{ECKO} retinas showed reduced EC proliferation *in vivo* (Figures S4H and S4I) and *in vitro* (Figure S6G), suggesting that a defect in proliferation might also account for the observed reduction in gap closure *in vitro*. Thus, to further characterize EC motility defects independent of proliferation, live imaging of random cell-motility tracks of individual non-dividing MBEs was performed. While control MBEs display significantly enhanced random movement upon VEGF stimulation, YAP/TAZ-silenced MBEs failed to increase their movement in response to VEGF (Figures 4F and 4G). Consistent with a regulatory function on the expression of cytoskeleton-related genes upon VEGF stimulation, HBMECs with YAP/TAZ knockdown failed to form lamellipodia after VEGF stimulation (Figures S6H and S6I). As Rac1 activity has been linked to VEGF-mediated lamellipodia formation (Tan et al., 2008), these results suggest that Rac1 activity might be impaired in YAP/TAZ knockdown cells.

Finally, we also analyzed the effect of YAP/TAZ knockdown in VEGF-induced sprouting and tube formation. While VEGF induced significantly longer sprouts in control conditions (Figures 4H and 4I), it was unable to do so in HBMECs when YAP/TAZ were knocked down. VEGF-induced tube formation and branching was also inhibited in YAP/TAZ knockdown cells (Figures S6J–S6L).

As it was previously shown that supplementation of Ang2 could rescue the phenotype of YAP knockdown in HUVECs (Choi et al., 2015), and we observed reduced Ang2 expression in isolated brain ECs from YAP/TAZ^{ECKO} pups (Figure 4B), we tested whether Ang2 could rescue the basal sprouting phenotype in YAP/TAZ knockdown HBMECs. Indeed, Ang2 supplementation rescued this basal sprouting defect (Figure S6M). We next tested whether the addition of Ang2 could compensate for the lack of response to VEGF stimulation in YAP/TAZ knockdown HBMECs. Addition of Ang2 together with VEGF did not

(F) Single cell-motility tracks of MBEs transfected with control siRNA or YAP/TAZ siRNA and treated with VEGF for 12 hr. Migration origin was overlaid at the zero cross point.

(G) Quantification of the absolute migration of cells in (F) showing that VEGF-induced migration in MBEs was suppressed by YAP/TAZ knockdown. At least 50 cells per condition were quantified.

(H) Representative images of the bead-sprouting assay using HBMECs transfected with control siRNA or YAP/TAZ siRNA and treated with VEGF for 24 hr. Scale bars, 200 μm.

(I) Quantitative analysis of total sprout length showing that VEGF does not induce sprouting when YAP/TAZ are knockdown. Forty beads per condition from four independent experiments were quantified.

For (G) and (I), data represent mean ± SEM from 4 independent experiments (***p < 0.001; ns, not significant). See also Figure S6; Tables S1 and S2.

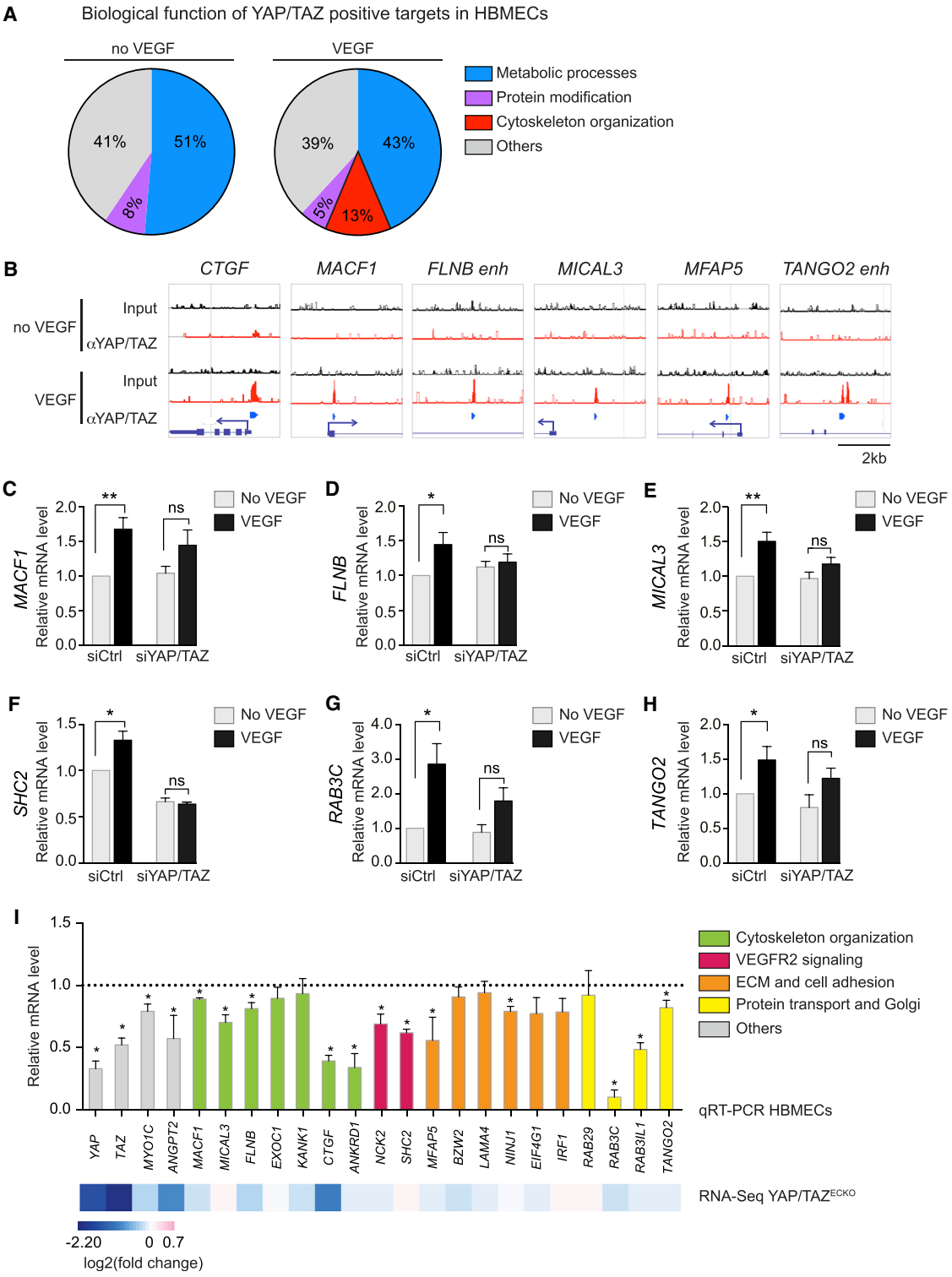

Figure 5. VEGF-Induced YAP/TAZ-Dependent Transcriptional Program Targets Primarily Cytoskeleton-Related Genes

(A) Diagram showing GO terms of the identified peaks upon ChIP-seq in non-stimulated or VEGF-stimulated for 6-hr HBMECs. Results show that upon VEGF stimulation a large group of YAP/TAZ target genes are responsible for cytoskeleton organization.

(B) Examples of gene peaks where YAP/TAZ bind to the promoter or enhancers (enh) upon VEGF stimulation.

(C–H) qRT-PCR validation of a set of VEGF-induced genes identified by YAP/TAZ ChIP-seq in HBMECs. Cells were transfected with control siRNA or YAP/TAZ siRNA and treated with VEGF for 12 hr.

(legend continued on next page)

rescue the inability of VEGF to induce sprouting in siYAP/TAZ transfected cells (Figures S6N and S6O), indicating that the observed phenotype is not just due to the reduced levels of Ang2 but that other molecular mechanisms involved in VEGF/VEGFR2 signaling are also affected.

Collectively, these data indicate that YAP/TAZ are required for the proper angiogenic response elicited by VEGF.

ChIP-Seq Analysis Reveals that YAP/TAZ Directly Control the Transcription of a Set of VEGF-Inducible Cytoskeleton Assembling Genes

As YAP/TAZ function as transcriptional co-factors, we performed chromatin immunoprecipitation sequencing (ChIP-seq) analysis using an anti-YAP/TAZ antibody with the aim to identify the direct target genes of YAP/TAZ under VEGF stimulation. By using peak calling methods (see STAR Methods), we found more YAP/TAZ binding sites in VEGF-stimulated HBMECs compared with non-stimulated ones. GO functional annotation indicated that in non-stimulated HBMECs YAP/TAZ were mainly bound to *cis* elements of metabolic-related genes (Figure 5A). However, after VEGF stimulation, YAP/TAZ binding appeared primarily onto a large group of genes involved in cytoskeleton remodeling (i.e., *MACF1*, *FLNB*, *MICAL3*, *CTGF*) (Figures 5A and 5B; Tables S3 and S4). In addition, other peaks identified corresponded to genes involved in cell adhesion/ECM remodeling (i.e., *NINJ1*, *MFAP5*), VEGF-VEGFR2 signaling (i.e., *NCK2*, *SHC2*) and vesicle-mediated protein transport (i.e., *RAB3C*, *RAB3IL1*) (Figure 5B and Table S3). These data suggest that a DNA binding complex containing YAP/TAZ controls the expression of those genes upon VEGF stimulation. To further confirm this observation, we performed qPCR analysis in control siRNA or YAP/TAZ siRNA transfected HBMECs that were stimulated with VEGF after overnight starvation. Indeed, qPCR analysis of several of those genes confirmed that YAP/TAZ are required for the VEGF-induced expression (Figures 5C–5H). Even in normal culture conditions, where VEGF is present at low concentrations, YAP/TAZ knockdown HBMECs presented reduced mRNA levels of most of those genes (Figure 5I). Consistently, most of the downregulated genes in YAP/TAZ knockdown HBMECs also matched with our RNA sequencing (RNA-seq) data from isolated brain ECs from YAP/TAZ^{ECKO} mice (Figure 5I, lower panel).

YAP/TAZ Silencing Impairs VEGFR2 Trafficking and VEGFR2 Downstream Signaling

A functional cytoskeleton is not only necessary to respond to migratory stimuli but is also required for intracellular protein trafficking (Allan et al., 2002; Rogers and Gelfand, 2000). In this sense VEGFR2 trafficking from and to the plasma membrane upon VEGF stimulation is crucial for proper signaling (Lanahan et al., 2010; Manickam et al., 2011; Tiwari et al., 2013; Yamada et al., 2014). Our RNA-seq data showed that *Myo1c* expression is significantly decreased by YAP/TAZ depletion in postnatal brain ECs (p_{adj} = 0.00015) (Table S1), which we also confirmed *in vitro* in YAP/TAZ knockdown HBMECs (Figure 5I). Interestingly, Myo1c is needed for the transport of a pool of VEGFR2 from the *trans*-Golgi network (TGN) to the plasma membrane, which is required to build up a full angiogenic response (Tiwari et al., 2013). This, together with the fact that many cytoskeleton remodeling genes were downregulated in YAP/TAZ^{ECKO} ECs and that some of the genes identified in our ChIP-seq analysis were classified as being involved in protein transport (i.e., *MACF1*, *RAB3C*, *RAB3IL1*; Figure 5I), led us to question whether VEGFR2 localization was altered in YAP/TAZ knockdown ECs. VEGFR2 staining in brain sections showed that in YAP/TAZ^{WT} ECs VEGFR2 was distributed evenly along the cells and part of it colocalized with IsoB4 (Figure 6A). In contrast, in ECs of YAP/TAZ^{ECKO} brains VEGFR2 mainly concentrated intracellularly (Figure 6A). Double immunostaining for VEGFR2 and a marker for the TGN in primary brain ECs isolated from YAP/TAZ^{WT} and YAP/TAZ^{ECKO} mice (where recombination was induced *in vitro* with 4-OH tamoxifen, Figure S7A) showed that VEGFR2 accumulates in the TGN in YAP/TAZ-depleted brain ECs (Figure S7B).

To further study the influence of YAP/TAZ on VEGFR2 localization, we used siCtrl or siYAP/TAZ transfected HBMECs. Although total VEGFR2 expression was not changed in YAP/TAZ knockdown cells, surface expression of VEGFR2 was significantly decreased (Figures 6B–6D). Consistently, the amount of VEGFR2 localized in the TGN was higher in YAP/TAZ knockdown cells compared with control ones (Figures 6E and 6F; Movies S1 and S2). According to previous findings (Gampel et al., 2006; Manickam et al., 2011; Tiwari et al., 2013), we also observed that VEGF stimulation led to VEGFR2 exit from the TGN (Figures 6G, 6H, and S7C); however, in YAP/TAZ knockdown HBMECs this process was strongly impaired (Figures 6G, 6H, and S7C).

To understand whether YAP/TAZ knockdown also results in reduced expression at the plasma membrane of other surface receptors, we analyzed Tie2, Neuropilin1 (NRP1), and LDL receptor-related protein 6 (LRP6) cellular distribution in siYAP/TAZ transfected HBMECs. While we only observed a trend toward reduced Tie2 and LRP6 expression at the plasma membrane (Figures S7D and S7E), NRP1 levels at the membrane were significantly reduced in siYAP/TAZ ECs compared with siCtrl ECs (Figures S7F and S7G), suggesting that YAP/TAZ might control cell-surface receptor trafficking differently.

We reasoned that if VEGFR2 presence at the plasma membrane is reduced in YAP/TAZ knockdown ECs, VEGFR2 activation and its downstream signaling should also be reduced. Consistent with this reasoning, we found that phosphorylation of certain tyrosine residues (Y1175, Y951, Y1212, and Y1054) required for VEGFR2 activation upon VEGF stimulation was strongly reduced (Figures 7A–7H). The downstream signaling events of VEGFR2, exemplified by pErk, pP38, pSrc, and pAkt, were also reduced in YAP/TAZ knockdown ECs

(I) Upper panel: relative mRNA levels (analyzed by qPCR) between HBMECs transfected with control (Ctrl) siRNA or YAP/TAZ siRNA and cultured under normal conditions showing the relative expression of some YAP/TAZ positive targets identified by ChIP-seq (colored bars), as well as other genes (gray bars). Note the downregulation of Ang2, used here as a positive control. Lower panel: heatmap of RNA-seq data showing that the same genes shown in the upper panel are also downregulated in primary isolated ECs of YAP/TAZ^{ECKO} mice.

For (C) to (I), data represent mean ± SEM of at least 3 independent experiments (*$p < 0.05$, **$p < 0.01$; ns, not significant). See also Figure S6; Tables S3 and S4.

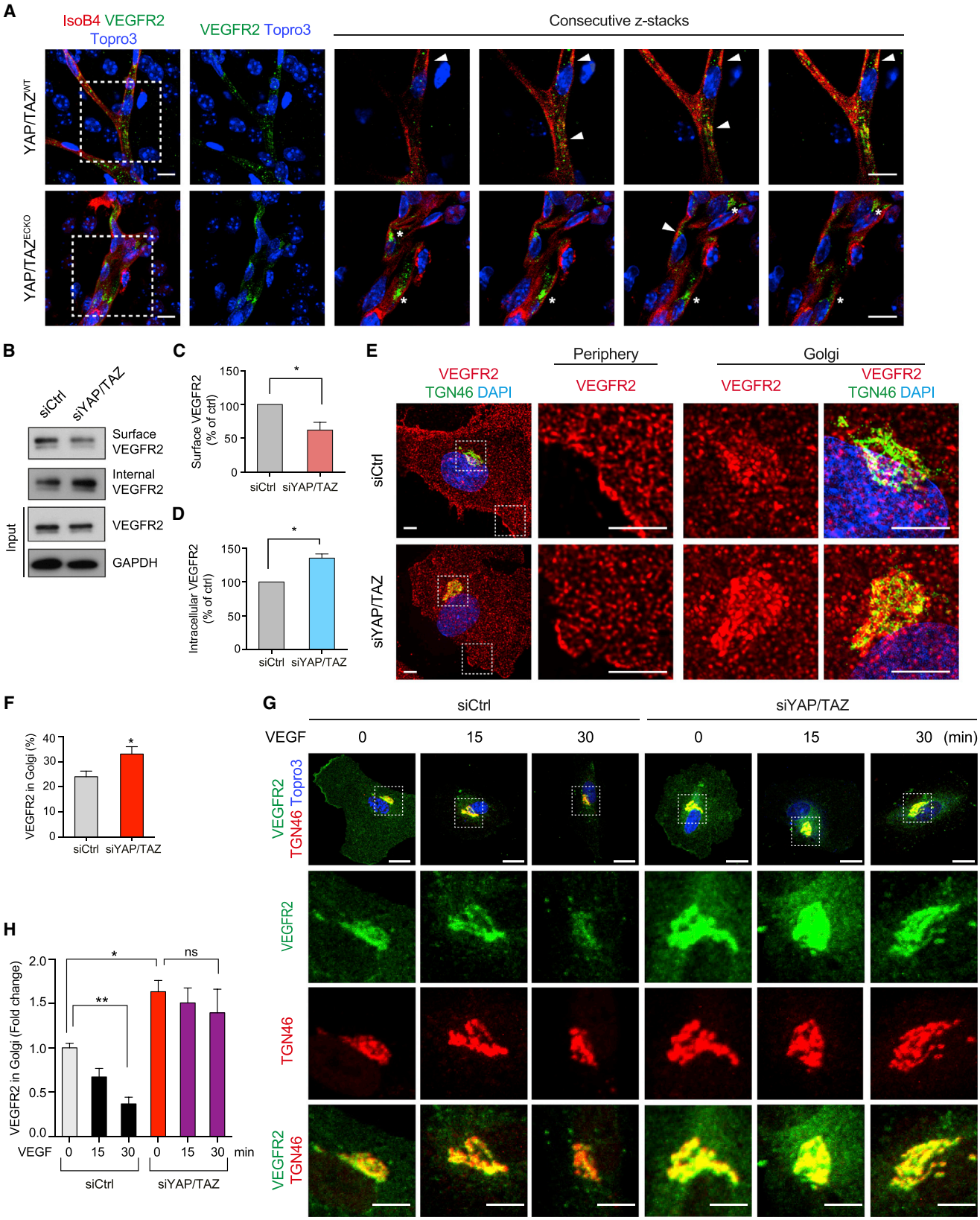

(legend on next page)

(Figures 7I–7P). We also observed that NCK2 and SHC2, two adaptor molecules recruited to VEGFR2 upon VEGF stimulation and required for proper VEGFR2 downstream signaling (Koch and Claesson-Welsh, 2012; Ratcliffe et al., 2002), were reduced in YAP/TAZ knockdown HBMECs (Figures 5F–5I). This suggests that besides the mislocalization of VEGFR2 at the plasma membrane, other mechanisms might partially contribute to the impaired VEGFR2 downstream signaling (such as the downregulated expression of *NCK2* and *SHC2*).

Collectively, these data support a model in which ECs require YAP/TAZ to regulate a transcriptional output for establishing a proper VEGFR2 trafficking process and signaling to ensure a full angiogenesis response to VEGF.

DISCUSSION

A remarkable trademark of YAP/TAZ is to control organ growth (Halder and Johnson, 2011). However, how they contribute to vascular growth and morphogenesis is almost unexplored. In this study we identify YAP/TAZ as a major regulator for transducing VEGF/VEGFR2 signaling into a specific transcriptional program, essential for blood vessel formation (Figure 7Q). We establish VEGF as a new extracellular cue that activates YAP/TAZ in ECs by modulating SFK and Rho GTPase activity, actin dynamics, and Lats1 activity (Figure 7Q).

A previous study showed retinal vascularization defects when YAP was knocked down by intraperitoneal injection of YAP siRNA during postnatal development (Choi et al., 2015). However, as that strategy results in a global knockdown of YAP and not an EC-specific one, it remained unknown whether the observed vascular phenotype was due to a direct effect in ECs or to a secondary effect from reducing YAP expression in other cell types. In this study, we show for the first time that EC-specific genetic deletion of YAP/TAZ leads to severe vascular defects during both embryonic and postnatal development. Embryonic deletion of YAP/TAZ in ECs results in embryo lethality, highlighting their essential role in the developing vasculature. Our data indicate that blood vessel defects can be attributed to reduced EC proliferation, migration, and sprouting. Interestingly, we also observed brain hemorrhages in YAP/TAZ^{ECKO} mice, suggesting that YAP/TAZ might additionally regulate EC permeability. While VE-cadherin at adherens junctions can regulate YAP transcriptional activity *in vitro* (Choi et al., 2015; Giampietro et al., 2015), it remains to be seen whether YAP/TAZ might control expression or function of EC junction molecules.

VEGF signaling ultimately results in the transcriptional control of a set of genes required for the angiogenic response of ECs (Wythe et al., 2013; Zhang et al., 2013). Here we link the VEGF and Hippo/YAP/TAZ signaling pathways and provide new mechanistic insights into how VEGF controls the transcription of a subset of those genes in brain ECs. Our ChIP-seq analysis identified that VEGF utilizes YAP/TAZ as co-transcription factors to control the expression of genes required for EC motility, including cytoskeleton organization, cell migration, and cell adhesion. Interestingly, while we observe that YAP/TAZ deletion has an effect in EC proliferation *in vivo*, this seems to be independent of their activation by VEGF, as genes involved in proliferation were not identified as YAP/TAZ targets upon VEGF stimulation. YAP/TAZ primarily bind to TEAD transcription factors (Zhao et al., 2008). In tumor cells TEAD4 cooperates with the transcription factor AP-1 to coordinate transcription of genes involved in cell motility (Liu et al., 2016). As TEAD4 and AP-1 were independently reported to be required for VEGF-induced angiogenesis (Jia et al., 2016; Liu et al., 2011), it is tempting to speculate that a similar mechanism exists in ECs where VEGF activates YAP/TAZ to coordinate a transcriptional response mediated by TEAD and AP-1. In addition, one of the main families of transcription factors activated by VEGF in ECs is the E26 transformation-specific (ETS) family, among them ERG (Wythe et al., 2013). Remarkably, in tumor cells ERG activates YAP-dependent transcriptional output (Nguyen et al., 2015), suggesting that perhaps in ECs a similar mechanism occurs.

The Notch, transforming growth factor β, bone morphogenetic protein, Wnt, and GPCR signaling pathways are also important for blood vessel development (Richard et al., 2001; Walchli et al., 2015). Each of these pathways has been reported to crosstalk with the Hippo signaling pathway and modulate YAP/TAZ activity in different cell types (Hansen et al., 2015). Although it still remains to be investigated, we could speculate that defects in those signaling pathways, together with the herein described defects in VEGF-VEGFR2 signaling and consequent impaired angiogenic response, might contribute to the overall YAP/TAZ^{ECKO} vascular phenotype. Moreover, this study, together with previous findings, points toward a role for YAP/TAZ as a major nexus that converge and integrate different

Figure 6. YAP/TAZ Are Required for Proper VEGFR2 Trafficking from the Golgi to the Plasma Membrane

(A) Representative images and consecutive z-stack insets of P12 brain vibratome sections (100 μm) stained for VEGFR2, IsoB4 (ECs), and Topro3 (nuclei), showing that in YAP/TAZ^{WT} ECs a part of VEGFR2 protein co-localizes with IsoB4 at the cell surface (arrowheads) while in YAP/TAZ^{ECKO} brain ECs VEGFR2 mainly concentrates intracellularly (asterisks). Scale bars, 20 μm (lower magnifications); 10 μm (insets).

(B) Surface biotinylation assay for VEGFR2 showing reduced levels of VEGFR2 at the plasma membrane in YAP/TAZ knockdown HBMECs compared with control ones.

(C and D) Quantification of cell surface (C) and intracellular VEGFR2 (D) of blots shown in (B); n = 3 independent experiments.

(E) High-resolution images of VEGFR2 localization in control and YAP/TAZ knockdown HBMECs. CD31 (EC marker) and TGN46 (*trans*-Golgi network [TGN] marker). Scale bars, 2 μm.

(F) VEGFR2 fluorescence intensity quantification at TGN; n ≈ 100 from 4 independent experiments.

(G) Representative images of VEGFR2 localization in the TGN of siCtrl and siYAP/TAZ transfected HBMECs, starved and stimulated with VEGF for the indicated time points. Scale bars, 10 μm (lower magnifications) and 20 μm (insets).

(H) Quantification of TGN-localized VEGFR2 (related to the total VEGFR2 fluorescence intensity in the cell) showing that VEGF stimulation results in VEGFR2 exit from TGN and that this is impaired in YAP/TAZ knockdown HBMECs; n ≈ 50 cells per condition from at least 4 independent experiments.

For (C), (D), (F), and (H), data are expressed as mean ± SEM (*p < 0.05, **p < 0.01; ns, not significant). See also Figure S7; Movies S1 and S2.

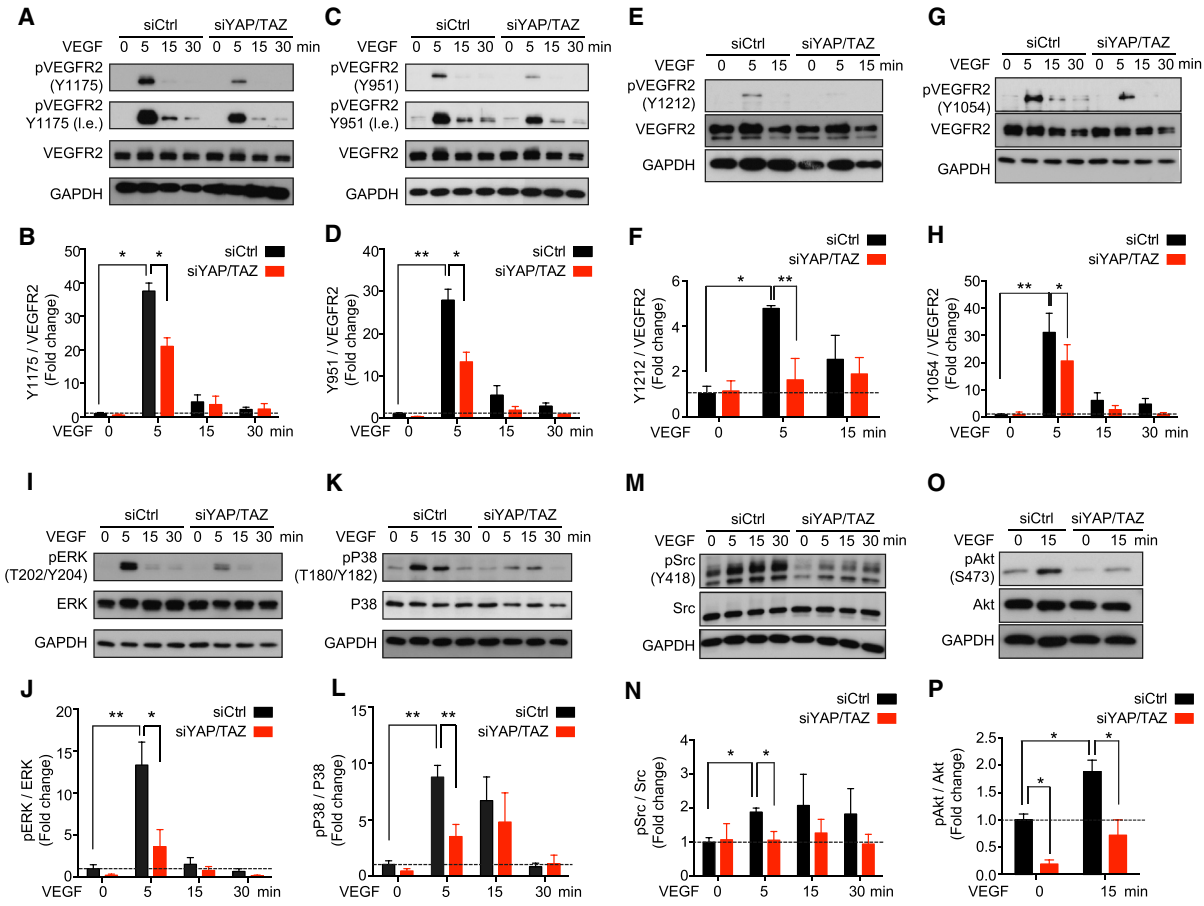

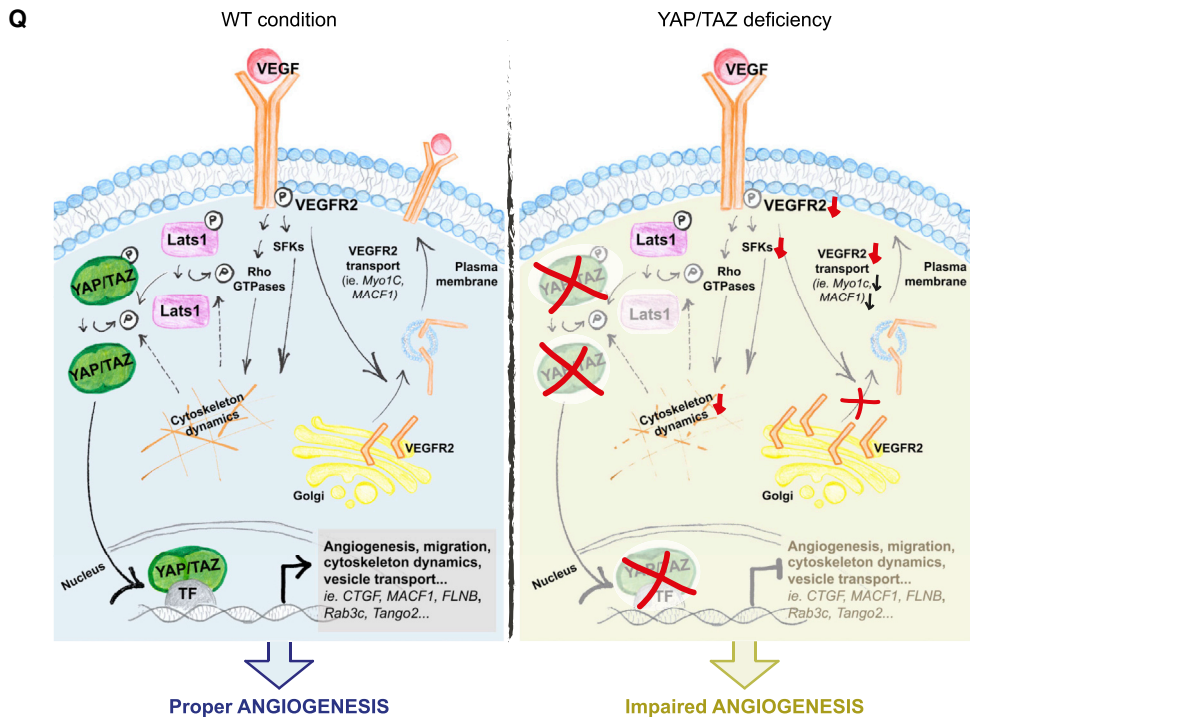

(legend on next page)

angiogenic stimuli into precise transcriptional programs in ECs. Further investigation is thus required to determine whether each independent stimulus results in a specific, or overlapping, YAP/TAZ-dependent transcriptional output, and whether this also varies between different EC types.

In this study, we find that in brain ECs YAP/TAZ control the expression of genes involved in cytoskeleton remodeling upon VEGF stimulation, and that ECs fail to remodel their cytoskeleton when stimulated with VEGF. YAP/TAZ also control the expression of certain genes involved in protein transport. In particular we find that MACF1 and Myo1c, two proteins that interact with actin and link the cytoskeleton to trafficking vesicles (Kakinuma et al., 2004; Tiwari et al., 2013), are under the control of YAP/TAZ. Cell-surface VEGFR2 is highly dynamic. Here we show that deletion of YAP/TAZ in ECs affects VEGFR2 protein trafficking from the TGN to the plasma membrane, most probably due to the combined downregulation of multiple genes involved in cytoskeleton remodeling and protein transport. Apart from the importance of VEGFR2 internalization upon VEGF stimulation (Simons et al., 2016), this study, together with previous evidence (Manickam et al., 2011; Tiwari et al., 2013), highlights the importance of the VEGF-induced delivery of VEGFR2 from the Golgi to the plasma membrane for a proper angiogenic response. It also provides further mechanistic insights into the regulation of this process. Thus, the described impaired VEGFR2 cellular distribution, trafficking, and signaling, and the impaired cytoskeleton dynamics provide part of the intricate molecular mechanisms that explain the angiogenesis defects in YAP/TAZ EC knockouts.

In conclusion, we propose that YAP/TAZ activity is required in ECs to build a transcriptional response that sustains VEGF signaling by controlling the expression of a set of genes that regulates actin cytoskeleton and participates in a positive feedback loop that delivers VEGFR2 from the TGN to the plasma membrane (Figure 7Q). Such a positive feedback loop would not be beneficial once formation of the vascular system has been completed, as this could lead to pathological situations, thus suggesting that in a quiescent endothelium YAP/TAZ, if expressed, should be localized to the cytosol. In support of this, our analysis of YAP/TAZ expression in ECs of adult mouse brain shows that they are localized in the cytosol, but that in a pathological condition such as brain tumor they relocalize to the nucleus. This study stimulates further interest in investigating whether targeting the identified downstream step of the VEGF signaling pathway might have similar, synergistic, or better outcome than solely trapping VEGF or blocking its receptors.

STAR★METHODS

Detailed methods are provided in the online version of this paper and include the following:

- KEY RESOURCES TABLE
- CONTACT FOR REAGENT AND RESOURCE SHARING
- EXPERIMENTAL MODEL AND SUBJECT DETAILS
- METHOD DETAILS
  - Cell Culture
  - Mouse Embryos and Postnatal Brains Tissue Processing
  - Immunofluorescence
  - Whole Mount Staining of Embryos and Yolk Sac
  - Hindbrain Dissection, Processing and Staining
  - Retina Dissection, Processing and Staining
  - Generation of Conditioned Medium from Spinal Cord Explants
  - Mouse Glioblastoma Model
  - Immunofluorescence of Cells in Culture
  - siRNA Transfection
  - Single Endothelial Cell Tracings
  - RNA Extraction and Quantitative Real-Time PCR Analysis
  - Luciferase Assays
  - Immunoprecipitation and Immunoblotting
  - Fibrin Gel Bead Sprouting Assay
  - Tube Formation Angiogenesis Assay
  - WST-1 Cell Proliferation Assay
  - Postnatal Brain EC Isolation RNA Sequencing and Gene Set Enrichment analysis (GSEA)
  - Gene Ontology Terms Network Visualization
  - ChIP-Seq
  - ChIP-Seq Data Analysis
  - Biochemical Quantification of Receptor Distribution
  - Image Processing
  - Quantification of VEGFR2 at the TGN
  - Immunoblotting for VEGFR2 Activation and Downstream Signaling
- QUANTIFICATION AND STATISTICAL ANALYSIS
- DATA AND SOFTWARE AVAILABILITY

SUPPLEMENTAL INFORMATION

Supplemental Information includes seven figures, five tables, and two movies and can be found with this article online at http://dx.doi.org/10.1016/j.devcel.2017.08.002.

Figure 7. YAP/TAZ Knockdown Results in Impaired VEGFR2 Downstream Signaling

(A, C, E, and G) Representative western blots for different VEGFR2 phosphorylation sites in HBMECs transfected with control or YAP/TAZ siRNA and stimulated with VEGF for the indicated time points, showing impaired VEGFR2 activation in YAP/TAZ depleted HBMECs.

(B, D, F, and H) Quantification of blots shown in (A), (C), (E), and (G); n = 3 (Y1175, Y951, Y1212) and 5 (Y1054) independent experiments.

(I, K, M, and O) Representative blots for pERK (I), pP38 (K), pSrc (M), and pAkt (O) in HBMECs treated as in (A), (C), (E), and (G), showing impaired VEGFR2 downstream signaling in YAP/TAZ knockdown cells.

(J, L, N, and P) Quantification of blots shown in (I), (K), (M), and (O); n = 3 independent experiments.

(Q) Working model showing that VEGF regulates YAP/TAZ activity via a mechanism that involves SFKs, Rho GTPases, cytoskeleton dynamics, and Lats1. The activation of YAP/TAZ is required to induce a transcriptional program that further transduces VEGF-induced angiogenesis effects. In the absence of YAP/TAZ (red crosses) VEGFR2 localization and signaling, as well as the YAP/TAZ-dependent transcriptional program, are impaired (red arrows depict the impaired steps identified in this study). Broken arrows depict the fact that the signaling steps in between the arrow are not yet identified.

For (B), (D), (F), (H), (J), (L), (N), and (P), data represent mean ± SEM (*$p < 0.05$, **$p < 0.01$).

AUTHOR CONTRIBUTIONS

Conceptualization, X.W. and C.R.d.A.; Investigation, X.W., A.F.V., G.S., I.M.M., Y.S., L.C., S.U., and M.M.; Writing – Original Draft, X.W. and C.R.d.A.; Writing – Review & Editing, A.F.V., I.M.M., R.K.J., M.M., T.S., T.F., and G.H.; Funding Acquisition, X.W., T.S., and C.R.d.A.; Resources, G.M.S., F.W., L.R., and R.K.J.; Supervision, T.F., G.H., and C.R.d.A.

ACKNOWLEDGMENTS

We thank Heike Adler and Melanie Richter for great technical assistance and all members of the C.R.d.A. laboratory for helpful discussions. We thank Prof. Adams for providing the Cdh5-(PAC)-CreERT2 mice, Prof. Johnson and Prof. Olson for providing the YAP/TAZ double floxed mice, Prof. Carmeliet for providing recombinant VEGF and VEGFR2 expression plasmids, PD. Dr. Liebner for providing MBEs, and Dr. Fischer for providing HUAECs. We thank Dr. Diz-Muñoz for helpful discussions. We thank the Nikon Imaging Center at Heidelberg University. C.R.d.A. is supported by ERC (ERC-StG-311367) and DFG grants FOR2325, SFB873, and RU 1990/1-1. X.W. was supported by an Alexander Von Humboldt postdoctoral fellowship. T.S. is supported by DFG grant SCHM 2560/3-1. G.H. is supported by the Flanders research foundation (FWO G.0954.16N). M.M. is supported by VLK (grant #419.052.173). The authors declare that they do not have any commercial interest in the subject of study. R.K.J. received consultant fees from Merck, Ophthotech, Pfizer, SPARC, SynDevRx and XTuit. R.K.J. owns equity in Enlight, SPARC, SynDevRx, and XTuit, and serves on the Board of Directors of XTuit and Boards of Trustees of Tekla Healthcare Investors, Tekla Life Sciences Investors, Tekla Healthcare Opportunities Fund, and Tekla World Healthcare Fund. No funding or reagents from these companies were used in this study.

Received: March 22, 2017
Revised: June 28, 2017
Accepted: August 2, 2017
Published: August 31, 2017

REFERENCES

Allan, V.J., Thompson, H.M., and McNiven, M.A. (2002). Motoring around the Golgi. Nat. Cell Biol. *4*, E236–E242.

Brigstock, D.R. (2002). Regulation of angiogenesis and endothelial cell function by connective tissue growth factor (CTGF) and cysteine-rich 61 (CYR61). Angiogenesis *5*, 153–165.

Carmeliet, P., Ferreira, V., Breier, G., Pollefeyt, S., Kieckens, L., Gertsenstein, M., Fahrig, M., Vandenhoeck, A., Harpal, K., Eberhardt, C., et al. (1996). Abnormal blood vessel development and lethality in embryos lacking a single VEGF allele. Nature *380*, 435–439.

Choi, H.J., Zhang, H., Park, H., Choi, K.S., Lee, H.W., Agrawal, V., Kim, Y.M., and Kwon, Y.G. (2015). Yes-associated protein regulates endothelial cell contact-mediated expression of angiopoietin-2. Nat. Commun. *6*, 6943.

Chung, A.S., and Ferrara, N. (2011). Developmental and pathological angiogenesis. Annu. Rev. Cell Dev. Biol. *27*, 563–584.

Dupont, S., Morsut, L., Aragona, M., Enzo, E., Giulitti, S., Cordenonsi, M., Zanconato, F., Le Digabel, J., Forcato, M., Bicciato, S., et al. (2011). Role of YAP/TAZ in mechanotransduction. Nature *474*, 179–183.

Fantin, A., Vieira, J.M., Plein, A., Maden, C.H., and Ruhrberg, C. (2013). The embryonic mouse hindbrain as a qualitative and quantitative model for studying the molecular and cellular mechanisms of angiogenesis. Nat. Protoc. *8*, 418–429.

Feng, J., Liu, T., Qin, B., Zhang, Y., and Liu, X.S. (2012). Identifying ChIP-seq enrichment using MACS. Nat. Protoc. *7*, 1728–1740.

Gampel, A., Moss, L., Jones, M.C., Brunton, V., Norman, J.C., and Mellor, H. (2006). VEGF regulates the mobilization of VEGFR2/KDR from an intracellular endothelial storage compartment. Blood *108*, 2624–2631.

Gao, T., He, B., Liu, S., Zhu, H., Tan, K., and Qian, J. (2016). EnhancerAtlas: a resource for enhancer annotation and analysis in 105 human cell/tissue types. Bioinformatics *32*, 3543–3551.

Gerhardt, H., Golding, M., Fruttiger, M., Ruhrberg, C., Lundkvist, A., Abramsson, A., Jeltsch, M., Mitchell, C., Alitalo, K., Shima, D., et al. (2003). VEGF guides angiogenic sprouting utilizing endothelial tip cell filopodia. J. Cell Biol. *161*, 1163–1177.

Giampietro, C., Disanza, A., Bravi, L., Barrios-Rodiles, M., Corada, M., Frittoli, E., Savorani, C., Lampugnani, M.G., Boggetti, B., Niessen, C., et al. (2015). The actin-binding protein EPS8 binds VE-cadherin and modulates YAP localization and signaling. J. Cell Biol. *211*, 1177–1192.

Halder, G., Dupont, S., and Piccolo, S. (2012). Transduction of mechanical and cytoskeletal cues by YAP and TAZ. Nat. Rev. Mol. Cell Biol. *13*, 591–600.

Halder, G., and Johnson, R.L. (2011). Hippo signaling: growth control and beyond. Development *138*, 9–22.

Hansen, C.G., Moroishi, T., and Guan, K.L. (2015). YAP and TAZ: a nexus for Hippo signaling and beyond. Trends Cell Biol. *25*, 499–513.

Himmels, P., Paredes, I., Adler, H., Karakatsani, A., Luck, R., Marti, H.H., Ermakova, O., Rempel, E., Stoeckli, E.T., and Ruiz de Almodovar, C. (2017). Motor neurons control blood vessel patterning in the developing spinal cord. Nat. Commun. *8*, 14583.

Huang da, W., Sherman, B.T., and Lempicki, R.A. (2009). Systematic and integrative analysis of large gene lists using DAVID bioinformatics resources. Nat. Protoc. *4*, 44–57.

Jia, J., Ye, T., Cui, P., Hua, Q., Zeng, H., and Zhao, D. (2016). AP-1 transcription factor mediates VEGF-induced endothelial cell migration and proliferation. Microvasc. Res. *105*, 103–108.

Kakinuma, T., Ichikawa, H., Tsukada, Y., Nakamura, T., and Toh, B.H. (2004). Interaction between p230 and MACF1 is associated with transport of a glycosyl phosphatidyl inositol-anchored protein from the Golgi to the cell periphery. Exp. Cell Res. *298*, 388–398.

Koch, S., and Claesson-Welsh, L. (2012). Signal transduction by vascular endothelial growth factor receptors. Cold Spring Harbor Perspect. Med. *2*, a006502.

Lam, M.T., Cho, H., Lesch, H.P., Gosselin, D., Heinz, S., Tanaka-Oishi, Y., Benner, C., Kaikkonen, M.U., Kim, A.S., Kosaka, M., et al. (2013). Rev-Erbs repress macrophage gene expression by inhibiting enhancer-directed transcription. Nature *498*, 511–515.

Lamalice, L., Le Boeuf, F., and Huot, J. (2007). Endothelial cell migration during angiogenesis. Circ. Res. *100*, 782–794.

Lanahan, A.A., Hermans, K., Claes, F., Kerley-Hamilton, J.S., Zhuang, Z.W., Giordano, F.J., Carmeliet, P., and Simons, M. (2010). VEGF receptor 2 endocytic trafficking regulates arterial morphogenesis. Dev. Cell *18*, 713–724.

Langmead, B., and Salzberg, S.L. (2012). Fast gapped-read alignment with Bowtie 2. Nat. Methods *9*, 357–359.

Liu, X., Zhao, D., James, L., Li, J., and Zeng, H. (2011). Requirement of the nuclear localization of transcription enhancer factor 3 for proliferation, migration, tube formation, and angiogenesis induced by vascular endothelial growth factor. FASEB J. *25*, 1188–1197.

Liu, X., Li, H., Rajurkar, M., Li, Q., Cotton, J.L., Ou, J., Zhu, L.J., Goel, H.L., Mercurio, A.M., Park, J.S., et al. (2016). Tead and AP1 coordinate transcription and motility. Cell Rep. *14*, 1169–1180.

Love, M.I., Huber, W., and Anders, S. (2014). Moderated estimation of fold change and dispersion for RNA-seq data with DESeq2. Genome Biol. *15*, 550.

Maere, S., Heymans, K., and Kuiper, M. (2005). BiNGO: a Cytoscape plugin to assess overrepresentation of gene ontology categories in biological networks. Bioinformatics *21*, 3448–3449.

Manickam, V., Tiwari, A., Jung, J.J., Bhattacharya, R., Goel, A., Mukhopadhyay, D., and Choudhury, A. (2011). Regulation of vascular endothelial growth factor receptor 2 trafficking and angiogenesis by Golgi localized t-SNARE syntaxin 6. Blood *117*, 1425–1435.

Mazzone, M., Dettori, D., Leite de Oliveira, R., Loges, S., Schmidt, T., Jonckx, B., Tian, Y.M., Lanahan, A.A., Pollard, P., Ruiz de Almodovar, C., et al. (2009). Heterozygous deficiency of PHD2 restores tumor oxygenation and inhibits metastasis via endothelial normalization. Cell *136*, 839–851.

Morin-Kensicki, E.M., Boone, B.N., Howell, M., Stonebraker, J.R., Teed, J., Alb, J.G., Magnuson, T.R., O'Neal, W., and Milgram, S.L. (2006). Defects in

yolk sac vasculogenesis, chorioallantoic fusion, and embryonic axis elongation in mice with targeted disruption of Yap65. Mol. Cell Biol. *26*, 77–87.

Murakami, M., Nakagawa, M., Olson, E.N., and Nakagawa, O. (2005). A WW domain protein TAZ is a critical coactivator for TBX5, a transcription factor implicated in Holt-Oram syndrome. Proc. Natl. Acad. Sci. USA *102*, 18034–18039.

Nakayama, M., Nakayama, A., van Lessen, M., Yamamoto, H., Hoffmann, S., Drexler, H.C., Itoh, N., Hirose, T., Breier, G., Vestweber, D., et al. (2013). Spatial regulation of VEGF receptor endocytosis in angiogenesis. Nat. Cell Biol. *15*, 249–260.

Nguyen, L.T., Tretiakova, M.S., Silvis, M.R., Lucas, J., Klezovitch, O., Coleman, I., Bolouri, H., Kutyavin, V.I., Morrissey, C., True, L.D., et al. (2015). ERG activates the YAP1 transcriptional program and induces the development of age-related prostate tumors. Cancer Cell *27*, 797–808.

Nishioka, N., Inoue, K., Adachi, K., Kiyonari, H., Ota, M., Ralston, A., Yabuta, N., Hirahara, S., Stephenson, R.O., Ogonuki, N., et al. (2009). The Hippo signaling pathway components Lats and Yap pattern Tead4 activity to distinguish mouse trophectoderm from inner cell mass. Dev. Cell *16*, 398–410.

Ohgushi, M., Minaguchi, M., and Sasai, Y. (2015). Rho-Signaling-directed YAP/TAZ activity underlies the long-term survival and expansion of human embryonic stem cells. Cell Stem Cell *17*, 448–461.

Piccolo, S., Dupont, S., and Cordenonsi, M. (2014). The biology of YAP/TAZ: hippo signaling and beyond. Physiol. Rev. *94*, 1287–1312.

Ratcliffe, K.E., Tao, Q., Yavuz, B., Stoletov, K.V., Spring, S.C., and Terman, B.I. (2002). Sck is expressed in endothelial cells and participates in vascular endothelial growth factor-induced signaling. Oncogene *21*, 6307–6316.

Richard, D.E., Vouret-Craviari, V., and Pouyssegur, J. (2001). Angiogenesis and G-protein-coupled receptors: signals that bridge the gap. Oncogene *20*, 1556–1562.

Rogers, S.L., and Gelfand, V.I. (2000). Membrane trafficking, organelle transport, and the cytoskeleton. Curr. Opin. Cell Biol. *12*, 57–62.

Shannon, P., Markiel, A., Ozier, O., Baliga, N.S., Wang, J.T., Ramage, D., Amin, N., Schwikowski, B., and Ideker, T. (2003). Cytoscape: a software environment for integrated models of biomolecular interaction networks. Genome Res. *13*, 2498–2504.

Simons, M., Gordon, E., and Claesson-Welsh, L. (2016). Mechanisms and regulation of endothelial VEGF receptor signalling. Nat. Rev. Mol. Cell Biol. *17*, 611–625.

Sun, Z., Li, X., Massena, S., Kutschera, S., Padhan, N., Gualandi, L., Sundvold-Gjerstad, V., Gustafsson, K., Choy, W.W., Zang, G., et al. (2012). VEGFR2 induces c-Src signaling and vascular permeability in vivo via the adaptor protein TSAd. J. Exp. Med. *209*, 1363–1377.

Tan, W., Palmby, T.R., Gavard, J., Amornphimoltham, P., Zheng, Y., and Gutkind, J.S. (2008). An essential role for Rac1 in endothelial cell function and vascular development. FASEB J. *22*, 1829–1838.

Tiwari, A., Jung, J.J., Inamdar, S.M., Nihalani, D., and Choudhury, A. (2013). The myosin motor Myo1c is required for VEGFR2 delivery to the cell surface and for angiogenic signaling. Am. J. Physiol. Heart Circ. Physiol. *304*, H687–H696.

van Nieuw Amerongen, G.P., Koolwijk, P., Versteilen, A., and van Hinsbergh, V.W. (2003). Involvement of RhoA/Rho kinase signaling in VEGF-induced endothelial cell migration and angiogenesis in vitro. Arterioscler. Thromb. Vasc. Biol. *23*, 211–217.

Vogel, J., Gehrig, M., Kuschinsky, W., and Marti, H.H. (2004). Massive inborn angiogenesis in the brain scarcely raises cerebral blood flow. J. Cereb. Blood Flow Metab. *24*, 849–859.

Wachsberger, P.R., Burd, R., Cardi, C., Thakur, M., Daskalakis, C., Holash, J., Yancopoulos, G.D., and Dicker, A.P. (2007). VEGF trap in combination with radiotherapy improves tumor control in u87 glioblastoma. Int. J. Radiat. Oncol. Biol. Phys. *67*, 1526–1537.

Wada, K., Itoga, K., Okano, T., Yonemura, S., and Sasaki, H. (2011). Hippo pathway regulation by cell morphology and stress fibers. Development *138*, 3907–3914.

Walchli, T., Wacker, A., Frei, K., Regli, L., Schwab, M.E., Hoerstrup, S.P., Gerhardt, H., and Engelhardt, B. (2015). Wiring the vascular network with neural cues: a CNS perspective. Neuron *87*, 271–296.

Wang, Y., Kilic, E., Kilic, U., Weber, B., Bassetti, C.L., Marti, H.H., and Hermann, D.M. (2005). VEGF overexpression induces post-ischaemic neuroprotection, but facilitates haemodynamic steal phenomena. Brain *128*, 52–63.

Wang, Y., Nakayama, M., Pitulescu, M.E., Schmidt, T.S., Bochenek, M.L., Sakakibara, A., Adams, S., Davy, A., Deutsch, U., Luthi, U., et al. (2010). Ephrin-B2 controls VEGF-induced angiogenesis and lymphangiogenesis. Nature *465*, 483–486.

Wythe, J.D., Dang, L.T., Devine, W.P., Boudreau, E., Artap, S.T., He, D., Schachterle, W., Stainier, D.Y., Oettgen, P., Black, B.L., et al. (2013). ETS factors regulate VEGF-dependent arterial specification. Dev. Cell *26*, 45–58.

Xin, M., Kim, Y., Sutherland, L.B., Qi, X., McAnally, J., Schwartz, R.J., Richardson, J.A., Bassel-Duby, R., and Olson, E.N. (2011). Regulation of insulin-like growth factor signaling by Yap governs cardiomyocyte proliferation and embryonic heart size. Sci. Signal. *4*, ra70.

Xin, M., Kim, Y., Sutherland, L.B., Murakami, M., Qi, X., McAnally, J., Porrello, E.R., Mahmoud, A.I., Tan, W., Shelton, J.M., et al. (2013). Hippo pathway effector Yap promotes cardiac regeneration. Proc. Natl. Acad. Sci. USA *110*, 13839–13844.

Xue, J., Schmidt, S.V., Sander, J., Draffehn, A., Krebs, W., Quester, I., De Nardo, D., Gohel, T.D., Emde, M., Schmidleithner, L., et al. (2014). Transcriptome-based network analysis reveals a spectrum model of human macrophage activation. Immunity *40*, 274–288.

Yamada, K.H., Nakajima, Y., Geyer, M., Wary, K.K., Ushio-Fukai, M., Komarova, Y., and Malik, A.B. (2014). KIF13B regulates angiogenesis through Golgi to plasma membrane trafficking of VEGFR2. J. Cell Sci. *127*, 4518–4530.

Yu, F.X., Zhao, B., Panupinthu, N., Jewell, J.L., Lian, I., Wang, L.H., Zhao, J., Yuan, H., Tumaneng, K., Li, H., et al. (2012). Regulation of the Hippo-YAP pathway by G-protein-coupled receptor signaling. Cell *150*, 780–791.

Zanconato, F., Cordenonsi, M., and Piccolo, S. (2016). YAP/TAZ at the roots of cancer. Cancer Cell *29*, 783–803.

Zhang, B., Day, D.S., Ho, J.W., Song, L., Cao, J., Christodoulou, D., Seidman, J.G., Crawford, G.E., Park, P.J., and Pu, W.T. (2013). A dynamic H3K27ac signature identifies VEGFA-stimulated endothelial enhancers and requires EP300 activity. Genome Res. *23*, 917–927.

Zhao, B., Ye, X., Yu, J., Li, L., Li, W., Li, S., Lin, J.D., Wang, C.Y., Chinnaiyan, A.M., Lai, Z.C., et al. (2008). TEAD mediates YAP-dependent gene induction and growth control. Genes Dev. *22*, 1962–1971.

Zhao, B., Li, L., Wang, L., Wang, C.Y., Yu, J., and Guan, K.L. (2012). Cell detachment activates the Hippo pathway via cytoskeleton reorganization to induce anoikis. Genes Dev. *26*, 54–68.

STAR★METHODS

KEY RESOURCES TABLE

REAGENT or RESOURCE	SOURCE	IDENTIFIER
Antibodies		
YAP/TAZ	Cell signaling	Cat#8418,RRID:AB_10950494
Histone H3-phospho (Ser10)	Cell signaling	Cat#9701, RRID:AB_331534
TER-119 Erythroid Antigen	R&D	Cat#MAB1125, RRID:AB_2297123
mouse CD31	BD Pharmingen	Cat#557355, RRID:AB_396660
CD31	Abcam	Cat#ab9498, RRID:AB_307284
Lyve1	Reliatech	Cat#103-PA50AG
Endoglin/CD105	R&D	Cat#MAB1320, RRID:AB_2098896
Collagen-IV	Biozol	Cat#CO20451
TGN46	santa cruz	Cat#sc166594, RRID:AB_2287347
TGN46	Biorad	Cat#AHP500G, RRID:AB_323104
mouse TGN46	R&D	Cat#MAB7944
YAP-Phospho (Ser127)	Cell signaling	Cat#4911, RRID:AB_2218913
YAP	Cell signaling	Cat#4912, RRID:AB_10694682
TAZ-phospho (Ser 89)	Santa cruz	Cat#sc-17610, RRID:AB_2216642
VEGFR2-phospho (Tyr1175)	Cell Signaling	Cat#2478, RRID:AB_331378
VEGFR2 (phospho Tyr951) (15D2)	Cell Signaling	Cat#4991, RRID:AB_331398
VEGFR2 phospho (Tyr1212) (11A3)	Cell Signaling	Cat#2477, RRID:AB_331374
P-VEGFR2 Tyr1059/1054	Cell Signaling	Cat#3817, RRID:AB_2132351
VEGFR2	Cell Signaling	Cat#2479, RRID:AB_2212507
GAPDH	Santa Cruz	Cat#sc-47724, RRID:AB_627678
β-Tubulin	Santa Cruz	Cat#sc-9104, RRID:AB_2241191
β-actin	Cell signaling	Cat#3700, RRID:AB_2242334
Src-Phospho (Tyr418)	invitrogen	Cat#44660G, RRID:AB_1500523
Src (36D10)	Cell Signaling	Cat#2109, RRID:AB_2106059
LATS1	Cell Signaling	Cat#3477, RRID:AB_2133513
LATS1-phospho (Ser909)	Cell signaling	Cat#9157, RRID:AB_2133515
LATS1 phospho-(Thr1079)	Cell signaling	Cat#8654, RRID:AB_10971635
Akt	Cell signaling	Cat#9272, RRID:AB_329827
Akt phospho (Ser473) (D9E)	Cell signaling	Cat#4060, RRID:AB_2315049
Erk1/2 p44/42	Cell signaling	Cat#9102, RRID:AB_330744
Erk1/2 phospho-p44/42 (T202/Y204)	Cell signaling	Cat#9106, RRID:AB_331768
p38 MAP kinase	Cell Signaling	Cat#9228, RRID:AB_490886
p-p38 MAP kinase	Invitrogen	Cat#36-8500, RRID:AB_2533281
Neuropilin1	Santa cruz	Cat#sc-7239, RRID:AB_2150835
Tie2	R&D	Cat#AF762, RRID:AB_2203220
Alexa Fluor 488-conjugated donkey anti-rabbit	Jackson ImmunoResearch	Cat#711-545-152, RRID:AB_2313584
Alexa Fluor 488-conjugated goat anti-rabbit	invitrogen	Cat#A11008, RRID:AB_143165
Alexa Fluor 488-conjugated donkey anti-sheep	Molecular Probes	Cat#A11015, RRID:AB_2534082
Alexa Fluor 568-conjugated goat anti-mouse	invitrogen	Cat#A11031, RRID:AB_144696
Alexa Fluor 568-conjugated goat anti-rabbit	invitrogen	Cat#A11031, RRID:AB_144696
Alexa Fluor 568-conjugated goat anti-rat	invitrogen	Cat#A11077, RRID:AB_10562719
Alexa Fluor 647-conjugated donkey anti-mouse	Jackson ImmunoResearch	Cat#715-605-151, RRID:AB_2340863
HRP donkey anti-rabbit antibody	Jackson ImmunoResearch	Cat#711-035-152, RRID:AB_10015282

(*Continued on next page*)

Continued

REAGENT or RESOURCE	SOURCE	IDENTIFIER
HRP donkey anti-mouse antibody	Jackson ImmunoResearch	Cat#715-035-150, RRID:AB_2340770
HRP donkey anti-goat antibody	Jackson ImmunoResearch	Cat#705-035-147, RRID:AB_2313587
Rabbit IgG	Dianova	Cat#DLN-013124
IgG from rat serum	Sigma Aldrich	Cat#18015
VEGFR2 blocking antibody	Bio X Cell	Cat#DC101, RRID:AB_1107766
Bacterial and Virus Strains		
8xGTIIC-luciferase	Addgene	Cat#34615
pRL-SV40	Promega	Cat#E2231
PC3.1	Prof.Peter Carmliet	N/A
VEGFR2 (flk)	Prof.Peter Carmliet	N/A
Chemicals, Peptides, and Recombinant Proteins		
Flt1/Fc	R&D	Cat#471-F1
VEGF	Prof.Peter Carmliet	N/A
C3	Cytoskeleton Inc.	Cat#CT04-A
PP3	Calbiochem	Cat#529574
PP2	Calbiochem	Cat#6506AP
Latrunculin B	Sigma Aldrich	Cat#L5288
Fibronectin	Sigma Aldrich	Cat#F0895
NHS-SS-biotin	Pierce	Cat#PG82077
4OH-Tamoxifen	Sigma	Cat#H7904
Alexa Flour 597-conjugated isolectinGS-IB4	Thermo Fisher	Cat#I21412
DAPI	Invitrogen	Cat#D1306
ToPRO-3 iodide	invitrogen	Cat#T3605
Phalloidin	Sigma Aldrich	Cat#P1951
Critical Commercial Assays		
WST1 cell proliferation assay	Sigma Aldrich	Cat#000000005015944001
μ-Slide Angiogenesis	ibidi	Cat#81506
Deposited Data		
Gene expression profile	NCBI Gebe Expression Omnibus	GSE94862
CHIP-Seq data	NCBI Gebe Expression Omnibus	GSE94862
Experimental Models: Cell Lines		
MBEs	Stefan liebner	N/A
HBMECs	Cell systems	Cat#ACBRI376
HUVECs	Promocells	Cat#C-12200
HEK293T	ATCC	Cat#CRL3216
CT26	ATCC	Cat#CRL2638
HUAECs	PD.Dr. Andreas Fisher	N/A
NIH3T3	ATCC	Cat#CRL1658
Experimental Models: Organisms/Strains		
NMRI nude mice	Charles River	N/A
CD1 mice	Janvier Labs and Charles River	N/A
C57/BL6	Janvier Labs and Charles River	N/A
Oligonucleotides		
Mouse Yap siRNA1: Sense 5'GCCAUGACUCAGGAUGGAGDTdT3'	Murakami et al., 2005, PNAS	N/A
Mouse Yap siRNA2: Sense 5'AGAAAGCUUUCUCACGUGGdTdT3'	Murakami et al., 2005, PNAS	N/A
Mouse Taz siRNA1: Sense 5'AAUCACCACAUGGCAAGACdTdT3'	Murakami et al., 2005, PNAS	N/A

(*Continued on next page*)

Continued

REAGENT or RESOURCE	SOURCE	IDENTIFIER
Mouse Taz siRNA2: Sense 5'AGAGAUACUUCCUUAAUCAdTdT3'	Murakami et al., 2005, PNAS	N/A
Human YAP siRNA: Sense 5'GACAUCUUCUGGUCAGAGA dTdT3'	Dupont et al., 2011, Nature	N/A
Human TAZ siRNA: Sense 5'ACGUUGACUUAGGAACUUU dTdT3'	Dupont et al., 2011, Nature	N/A
Mouse primers, see Table S5	This paper	N/A
Human primers, see Table S5	This paper	N/A
Software and Algorithms		
NIH ImageJ	NIH	N/A
Cytoscape 3.4.0	Shannon et al., 2003	N/A
Bowtie2 software	Langmead and Salzberg, 2012	http://bowtie-bio.sourceforge.net/bowtie2/index.shtml
MACS2 v1.4.2	Feng et al., 2012	N/A
Prism 6.0 software	GraphPad	N/A
Huygens Remote Manager v3.2.1	University Heidelberg	http://www.huygens-rm.org/wp/

CONTACT FOR REAGENT AND RESOURCE SHARING

Further information and requests for reagents may be directed to and will be fulfilled by the Lead Contact, Carmen Ruiz de Almodóvar (carmen.ruizdealmodovar@bzh.uni-heidelberg.de)

EXPERIMENTAL MODEL AND SUBJECT DETAILS

All experimental protocols of mice were approved by the local authorities and animal welfare officers and in accordance with the NIH "Guide for the Care and Use of Laboratory Animals". Generation of $YAP^{fl/fl}$;$TAZ^{fl/fl}$ mice has been described previously (Xin et al., 2011, 2013). $YAP^{fl/fl}$;$TAZ^{fl/fl}$ mice were crossed with Cdh5(PAC)$^{CreERT2/+}$ mice (Wang et al., 2010) to specifically delete YAP/TAZ in the endothelium. Embryonic Cre recombination was induced by intraperitoneal injections of pregnant females with 200μl Tamoxifen (10mg/mL, prepared in ethanol/peanut oil followed by ethanol evaporation). Postnatally, Cre recombination was induced by intragastric injection of 50μl tamoxifen (1mg/mL). The TgN(NSEVEGF)1651 (V1) (NSE-$VEGF^{tg}$) mouse line was described previously (Vogel et al., 2004; Wang et al., 2005), wild type littermates (WT) were used as controls. Wild type CD1 and C57Bl/6 mice were purchased from Janvier Labs and Charles Rivers. All experiments were performed in accordance to local authorities and animal welfare officers of Baden-Wuerttemberg (Germany).

METHOD DETAILS

Cell Culture

Human brain microvascular endothelial cells (HBMECs) were purchased from Cell Systems (Kirkland, Washington). Mouse brain endothelioma cells (MBEs) were a gift from PD. Dr. Stefan Liebner (University hospital Frankfurt). Human umbilical vein endothelial cells (HUVECs) were purchased from PromoCell (Heidelberg, Germany). Human umbilical aortic endothelial cells (HUAECs) were a gift from PD. Dr. Andreas Fischer. HEK293T, NIH3T3 and CT26 were obtained from ATCC (Manassas, VA). Endothelial cells were maintained in 0.1% porcine gelatin coated flasks. MBEs were cultured in MCDB-131 medium (Life Technology), supplemented with 15%FBS, 100 U/mL penicillin and 100 μg/mL streptomycin, 0.1mg/mL Heparin (Sigma Aldrich), MEM non-essential amino acid solution (Sigma Aldrich) and 0.5mg/mL endothelial cell growth supplement from bovine neural tissue (Sigma Aldrich). HBMECs, HUVECs and HUAECs were cultured in Endopan 3 Kit for endothelial cells (PAN-Biotech, GmbH, Aidenbach, Germany) supplemented with 10% FBS, 100 U/mL penicillin and 100 μg/mL streptomycin (both Gibco® by Life Technologies, Grand island, NY, USA). For studying the signaling of YAP/TAZ activation and signaling of VEGFR2 activation, all cells were starved overnight in serum free medium before VEGF (50ng/mL) stimulation or other treatments (i.e. addition of recombinant proteins, blocking antibodies, chemicals, FBS (10%) or SC-CM). For analyzing phosphorylation status of Lats1, YAP/TAZ and nuclear localized YAP/TAZ after VEGF, 50ng/mL VEGF were added to starved cells for 2 hours unless mentioned otherwise. For checking *Ctgf* and *Cyr61* RNA expression, 50ng/mL VEGF or other treatments (FBS (10%) or SC-CM) were added to starved cells for 6 hours. For analyzing l*amellipodia* formation, starved cells were treated with 50ng/mL VEGF for 30 min. Quantification of *lamellipodia* was done as previously described (Mazzone et al., 2009). For Figure 5C–5H, starved cells were treated with 50ng/mL VEGF for 12 hours. Treatment with inhibitors or blocking solution: Flt1/Fc (1μg/mL), α-VEGFR2 (5μg/mL, pretreat for 2hours), Latrunculin B (1μg/mL pretreat for 30mins,

unless mentioned otherwise), PP3/PP2 (10μM, pretreat for 1hour), C3 (2μg/mL, pretreat for 4 hours). For inducing Cre activity in freshly isolated brain endothelial cells, cells were treated with 5μM 4-hydroxytamoxifen (4-OHT) for 48 hours. HEK293T, NIH3T3 and CT26 were cultured in Dulbecco Modified Eagle's Medium containing 10% FBS. HBMECs from passages 5 to 10 and HUVECs from passages 3 to 5 were used for the experiments. In general, similar results were observed when testing the different endothelial cell types used in this study.

Mouse Embryos and Postnatal Brains Tissue Processing

To analyze the vasculature of mouse embryos, embryos were collected at different embryonic stages (E10.5 to E14.5) and fixed by 4% paraformaldehyde/PBS at 4°C overnight. Afterwards, they were transferred to 30% sucrose/PBS at 4°C overnight and subsequently embedded in OCT and stored at -80°C. Serial 40 μm-thick transverse sections were cut using a cryostat (MICROM HM560) and collected on SuperFrost® Plus slides (Menzel-Glaeser, Braunschweig, Germany). To check the vasculature of post-natal mouse brains, the samples were fixed in 4%PFA at 4°C overnight, afterwards 100μm coronal vibratome sections were made.

Immunofluorescence

Vibratome or cryosections were washed, permeabilized in PBS containing 0.3% TritonX-100 then blocked in PBS solution with 2%BSA, 0.3% TritonX-100 for 1h, and incubated with primary antibodies (YAP/TAZ, 1:200; TER-119, 1:100; mouse CD31, 1:100; mouse Lyve-1, 1:200; VEGFR2, 1:100). After washing, sections were incubated with secondary antibody for 2 hours. Images were collected on a confocal microscope (LSM 510, Carl Zeiss). For checking vasculature defects, quantification was done blind to mouse genotype.

Whole Mount Staining of Embryos and Yolk Sac

For whole embryo staining, freshly dissected embryos were fixed in 4% PFA at 4°C overnight and dehydrated and rehydrated in graded methanol series. Embryos were then washed with PBS and blocked in 0.5% TritonX-100, 2% milk. Anti-Endoglin (1:100) was diluted in blocking solution and incubated overnight at 4°C with rocking. After washing, embryos were incubated with secondary antibody (1:400), 4°C overnight. Embryos were mounted with Mowiol mounting medium (Sigma) and imaged on a confocal fluorescence microscope (LSM 510, Carl Zeiss).

For yolk sac staining, yolk sacs were freshly dissected and fixed in 4% PFA at 4°C overnight. After fixation, yolk sacs were washed with 0.3% TritonX-100 TBS, and blocked in 5% normal donkey serum (Dianova), 0.2% BSA, 0.3% TritonX-100 TBS. Endoglin (1:200) was diluted in blocking solution and incubated at 4°C overnight. After washing with 0.3% TritonX-100 TBS (4x 15 min), yolk sacs were incubated with secondary antibody (1:400) for 4 hours. Images were taken on a confocal microscope (LSM 510, Carl Zeiss). Number of branches was counted manually. Quantification was done blind to mouse genotype.

Hindbrain Dissection, Processing and Staining

Wild type E11.5 and E12.5 embryo hindbrains were dissected as previously described (Fantin et al., 2013), followed by 2h fixation in 4%PFA on ice. After washing, the samples were blocked in 2%BSA with 0.3% Triton X100 overnight at 4°C in 2.0-ml round-bottomed Safe-Lock tubes. Samples were then incubated overnight with primary antibody (YAP/TAZ, 1:200). After washing, hindbrains were incubated with Alexa Fluor 488-conjugated donkey anti-rabbit antibody (1:400) and Alexa Fluor 597-conjugated isolectinGS-IB4 solution (1:250) at 4°C overnight. Nuclei were stained with Topro3 (1:1000) for 15 min. Flat-mounted hindbrains were analyzed using a confocal fluorescence microscope (LSM 510; Carl Zeiss).

Retina Dissection, Processing and Staining

Mice were sacrificed and eyes were enucleated in PBS. The eyes were fixed in 4% PFA/PBS for 1h at 4°C. Retinas were dissected, washed with PBS and permeabilized with PBS containing 1% Triton X-100 for 1h. Then, they were incubated overnight in 0,1% tween, 10% normal goat serum (NGS, Dianova) in PBS at 4 °C. After, the retinas were incubated with primary antibodies (YAP/TAZ, 1:100) and after washing with PBS, they were incubated overnight with Alexa Fluor 488-conjugated goat anti-rabbit antibody (1:100) and Alexa Fluor 597-conjugated isolectinGS-IB4 solution (1:100) at 4°C. Nuclei were stained with Topro3 (1:1000) for 15 min. For staining Collagen IV (Col IV) and phospho-Histone H3 (pH3), retinas were blocked and permeabilized with 0.5% Triton-X-100, 10%NGS in PBS for 1.5h at RT. After that, they were incubated with primary antibodies (Col IV or pH3, 1:100) in 10%NGS, 1%BSA, 0.2% tween in PBS overnight at 4°C. After washing, retinas were incubated with corresponding secondary antibodies and Alexa Fluor 597-conjugated isolectinGS-IB4 solution (1:250) for 2h at RT. Flat-mounted retinas were analyzed using a confocal fluorescence microscope (LSM 510; Carl Zeiss). Quantification was done blind to mouse genotype.

Generation of Conditioned Medium from Spinal Cord Explants

Spinal cord explants from E11.5 wild type mice were isolated via open book preparation and cultured in 3D collagen type I (Corning) in neurobasal culture medium (Life technologies) with B-27 Supplement (Life technologies). Explant conditioned medium or control medium (without explants) were collected after 48h and directly applied to ECs.

Mouse Glioblastoma Model

The human glioblastoma (GBM) cell line U-87 MG from the American Type Culture Collection (ATCC) was used. For the cultured cells a contamination and authentication test was done by the Multiplexion GmbH (Heidelberg, Germany) company. The cell line was cultured under adherent conditions with Dulbeccos's Modified Eagles's Medium (DMEM), which was supplemented with 10% fetal bovine serum (FBS) and 1% penicillin-streptomycin. 1μl cell suspension, containing 50,000 tumor cells, was injected cortically 500μm deep into the brain of 8-10 weeks old male NMRI nude mice (Charles River). 34 days after tumor injection the animals were sacrificed and the brains were snap frozen and 10μm brain slices were cut at the cryomicrotome (CM 1950, Leica Mikrosysteme Vertrieb GmbH).

Immunofluorescence of Cells in Culture

For YAP/TAZ staining, endothelial cells were seeded in cover slips coated with fibronectin. After treatment, cells were fixed with 4% PFA/PBS for 15min at RT. Afterwards, cells were permeabilized with 0.2% Triton X-100 PBS, blocked in 2%BSA, 0.2% Triton X-100 PBS, and incubated with primary antibodies (YAP/TAZ, 1:400; mouse CD31, 1:200; human CD31, 1:200). After washing, cells were incubated with secondary antibodies. Phalloidin (1:400) was used together with secondary antibodies. Images were acquired by confocal microscope (Zeiss LSM 510). More than 12 fields of view from at least three independent experiments were randomly chosen. Cells presenting preferential nuclear YAP/TAZ localization, equal nuclear or cytoplasmic, or mainly cytoplasmic YAP/TAZ localization were counted blindly. For VEGFR2 staining, endothelial cells were plated in cover slips coated with 0.1% gelatin. After treatment, cells were fixed in 4% PFA/PBS and permeabilized with 0.2% % Triton X-100 PBS, blocked in 2%BSA, 0.2% Triton X-100 PBS, and incubated with primary antibodies (VEGFR2, 1:200; TGN46, 1:200; CD31, 1:100). After washing, cells were incubated with secondary antibodies.

siRNA Transfection

The sequences of siRNA were as previously described (Dupont et al., 2011; Murakami et al., 2005). MBEs or HBMECs were seeded in a 6 well plate, after 16h 70-80% confluent cells were transfected with control siRNA or siRNA for YAP/TAZ (see Key Resources Table) using Oligofectamine (Life technology) according to the manufacturer's instructions. The final concentration of siRNA solution was 200nM. MISSION® siRNA Universal Negative Control (Sigma-Aldrich) was used as control.

Single Endothelial Cell Tracings

Transfected endothelial cells were plated on 6 well plates and stimulated with 50ng/mL VEGF or control vehicle. Phase contrast images of 15 fields of view per experiment were acquired every 10 min over the course of 12h using an inverted NikonTi microscope (with a Nikon Plan Fluor 10x NA 0.3 objective) equipped with an environmental box from Oko Lab for temperature, CO_2 and humidity control. Endothelial cell migration was traced automatically using NIS Elements 4.5 software.

RNA Extraction and Quantitative Real-Time PCR Analysis

ECs in culture were harvested for RNA extraction using Trizol reagent (Life Technology) or mini RNA extraction kit (Qiagen). RNA samples were reverse-transcribed to complementary DNA (cDNA) using Maxima Reverse Transcriptase (Thermo Scientific) or SuperScript VILO cDNA Synthesis Kit (Invitrogen). qRT-PCR was performed using Fast SYBR Green Master Mix (Thermo Scientific) and the 7300 real-time PCR system (Applied Biosystems). GAPDH was used as internal control. All qPCR results were obtained from at least 3 biological repeats.

Luciferase Assays

8xGTIIC-luciferase (80ng/cm^2, Addgene) plasmid was transfected together with pRL-SV40 (10ng/cm^2, Promega), PC3.1 or VEGFR2 expression plasmid using lipofectamine 2000 (Life technologies). 30h after transfection, cells were starved in serum free medium overnight, followed by 50ng/mL VEGF stimulation for 24h. Cell lysates were subjected to Dual luciferase assay system (Promega) reagents. Results were measured in Perkin Elmer luminometer.

Immunoprecipitation and Immunoblotting

Co-IP assays for detecting p-TAZ were performed by using Crosslink Magnetic IP and Co-IP Kit (Pierce) according to the manufacturer's instructions. TAZ was immunoprecipitated using YAP/TAZ antibody (Cell Signaling). pTAZ was detected by using anti-TAZ-phospho (Ser89) (Santa Cruz). For detecting p-Lats in Figure 2J, cells were lysed using mild lysis buffer (20 mM Tris at pH 7.5, 150 mM NaCl, 5 mM EDTA, 1% NP-40, 10% Glycerol, 1X protease inhibitor cocktail and 1X phosphatase inhibitor (Roche)). Cell lysates were centrifuged for 15 min, and supernatants were used for immunoprecipitation. Anti-Lats1 antibody (Cell signaling) was incubated with the supernatant overnight on a rotor, and protein A/G –magnetic beads (Pierce) were added in for 2 more hours. Immunoprecipitates were washed one time with lysis buffer and two more times with Tris-HCL buffer, and proteins were eluted with SDS sample buffer. phospho-Lats was detected by using anti Lats1 phospho-(Ser909) and anti- Lats1 phospho-(Thr1079).

Fibrin Gel Bead Sprouting Assay

Fibrin gel bead sprouting assay was performed as previously described (Choi et al., 2015). Briefly, cytodex 3 microcarrier beads (GE Healthcare) were coated with siRNA-transfected HBMECs (mixed at 200 cells per bead), and embedded in 2 mg/mL fibrin

gels in 24-well plates by mixing 2 mg/mL fibrinogen (Calbiochem) in PBS, 0.625 Units/mL thrombin (Sigma-Aldrich), and 0.15 Units/mL aprotinin (Sigma-Aldrich). HBMECs-coated beads were cultured in 2%FBS growth factor-free Endopan medium with the indicated stimulation. After 24 hours the culture was fixed with 4%PFA for 15min, blocked in 1%BSA, 0.2% TritonX-100-PBS and incubated with 1μg/mL Phalloidin (Sigma-Aldrich) 2h. Confocal images were taken with the Zeiss LSM 510 microscope and sprout length analyzed by NIH ImageJ.

Tube Formation Angiogenesis Assay

Tube formation assays were performed as previously described (Himmels et al., 2017), by using μ-Slide Angiogenesis (ibidi). Briefly, siRNA transfected HBMECs were seeded on growth factor reduced matrigel (BD Bioscience)-coated Ibidi slides in 2%FBS growth factor-free Endopan medium, with or without VEGF (50ng/mL, 4 hours). Images were acquired by using a Zeiss Axiovert 200 M microscope. Images were analyzed with NIH ImageJ software.

WST-1 Cell Proliferation Assay

HBMECs were plated in 96 well plate, after 16h were transfected with control siRNA or siRNA for YAP/TAZ at 200nM. After 36 hours, cells were starved overnight, and stimulated with VEGF (50ng/mL, 24 hours). WST-1 assay was performed according to the manufacturer's instructions by using Cell Proliferation Reagent WST-1 (Sigma-Aldrich).

Postnatal Brain EC Isolation RNA Sequencing and Gene Set Enrichment analysis (GSEA)

Postnatal mouse brain ECs were isolated by magnetic cell separation method (Miltenyi Biotec) according to the manufacturer's instructions. Briefly, freshly dissected postnatal brains were disassociated, followed by myelin depletion, CD45+ cells depletion, and CD31+ cells selection. 4 YAP/TAZ^{WT} pups and 3 YAP/TAZ^{ECKO} pups from 2 litters were used for this experiment. Total RNA was isolated by using mini RNA isolation kit (Qiagen). Sequencing was performed by Cell Networks facility (Heidelberg, Germany) on Illumina Hiseq platform. Sequencing reads were mapped by Tophat2 software (version 2.0.14) to version mm10 of the human genome. Expression changes between the YAP/TAZ^{WT} and YAP/TAZ^{ECKO} group was calculated with DESeq2 package (Love et al., 2014). Expression values were rlog transformed. Sequencing data have been deposited in the Gene Expression Omnibus (GEO) database with accession codes GSE94862. For Gene set enrichment analysis, VEGF regulated transcriptome data in HUVECs was obtained via accession number GSE41166 and the corresponding mouse transcripts were mapped using Ensmbl Gene IDs.

Gene Ontology Terms Network Visualization

Network generation was performed as previously described (Xue et al., 2014) with slightly modification. Briefly, 137 down- and 119 up-regulated genes (absolute $\log_2$ fold-change >0.5, P_{adj} <0.05) in YAP/TAZ^{ECKO} compared to YAP/TAZ^{WT} were applied into Cytoscape 3.4.0 (Shannon et al., 2003) by using BiNGO plugin (Maere et al., 2005), respectively. Networks were visualized in a force-directed layout.

ChIP-Seq

Chromatin immunoprecipitation was performed as previously described (Lam et al., 2013). Briefly, HBMECs cultured in subconfluent status were starved overnight, and treated with or without 50ng/mL VEGF for 6h. Cells were then fixed with 1% formaldehyde (Sigma) in medium for 10min at RT, and lysed in 1%SDS lysis buffer. Chromatin was sheared to approximately 200bp fragments by using Covaris S220X. Sheared chromatin was incubated with anti-YAP/TAZ antibody overnight at 4°C and further incubated with Protein A/G magnetic beads (Pierce) for 2h. Chip'd DNA from 2 immunoprecipitations were pooled to generate libraries by ThruPLEX DNA-seq Kit (Rubicon). Sequencing was performed by Cell Networks facility (Heidelberg, Germany) on Illumina Hiseq platform. Sequencing data have been deposited in the Gene Expression Omnibus (GEO) database with accession code GSE94862.

ChIP-Seq Data Analysis

Sequencing reads were mapped by Bowtie2 software (version 2.2.5) to version hg38 of the human genome. MACS2 v1.4.2 (Feng et al., 2012) were used to call peaks using input from each sample as control. Peaks in the centromeres, in repeat regions, and in the blacklisted regions from ENCODE project were filtered out. To get a list from the affected genes, we paired the peaks within ±1000bp from transcriptional start sites (TSS), as listed in Table S3. Peak coordinates were transformed to hg37 using UCSC liftover service to use them in the Enhancer Atlas database (Gao et al., 2016). The predicted target genes were used to perform Gene Ontology analysis (Huang da et al., 2009) for generating Figure 5A. The list of the Biological Process category enriched in direct positive YAP/TAZ targets under VEGF stimulation or non-stimulated condition could be assigned to three broad categories: metabolic process, cytoskeleton organization and protein modification (Table S4).

Biochemical Quantification of Receptor Distribution

Biotinylation of VEGFR2, Tie2, LRP6 and NRP1 was performed as described previously (Gampel et al., 2006). Briefly, HBMECs transfected with YAP/TAZ siRNA or control siRNA were washed, and labeled using a membrane impermeant biotinylation reagent (NHS-SS-Biotin, Pierce). The unlabeled biotin was quenched by washing once with TBA (25mM Tris, PH8.0; 137mM NaCl; 5mM KCl; 2.3mM $CaCl_2$; 0.5mM $MgCl_2$, and 1mM Na_2HPO_4), followed by 3 more washes with PBS. Cells were lysed using mild lysis buffer (20mM Tris, PH7.5; 125mM NaCl; 10% glycerol; 1% NP40) with 1X protease inhibitor cocktail and 1X phosphatase inhibitor (Roche).

Cell lysates were centrifuged and a sample from the supernatant was taken as representation of total cellular receptor. Streptavidin-magnetic beads (Pierce) were used to pull down surface receptors. The negative flow from the pull down represents the internal receptor. Immunoblotting was performed using standard protocol. Representative blot is shown from 3 independent biological repeats.

Image Processing

Stained cells for VEGFR2 were analyzed using an ERS-6 spinning disk confocal microscope. Images were taken with a 100x objective (Nikon Plan Apo λ 100x NA 1.45) and processed with Huygens deconvolution Software (Huygens Professional, Scientific Volume Imaging). Images were obtained from z-stacks consisting of 30-50 optical slices, taken at 0.13μm. A nonblind deconvolution method was used on the image stacks for the high-resolution images before 3D reconstruction. Further parameters used in the Huygens deconvolution software were: NA of the objective (1.45), refractive index of the embedding medium (1.4) and refractive index of the lens immersion medium (1.515). All other parameters, like signal-to-noise ratio, were set between 25-30. Videos were generated in NIH ImageJ software with the 3D Project tool.

Quantification of VEGFR2 at the TGN

For quantifying the percentage of VEGFR2 localized in the *trans*-Golgi network (TGN) Anti-TGN46 antibody was used to stain the TGN area. The integrated fluorescence intensity of total VEGFR2 in the cell or Golgi-localized VEGFR2 was quantified by ImageJ software. For each condition, 24 images containing approximately 100 cells from 5 independent biological experiments were analyzed. For quantifying differences in TGN VEGFR2 content, the mean fluorescence intensity was used. Approximately 100 cells from 5 independent biological experiments were analyzed.

Immunoblotting for VEGFR2 Activation and Downstream Signaling

HBMECs transfected with YAP/TAZ siRNA or control siRNA were starved, and stimulated with 50ng/mL VEGF for indicated time points. Cells were then washed with ice cold PBS and lysed in RIPA buffer containing 1X protease inhibitor cocktail and 1X phosphatase inhibitor (Roche). Immunoblotting was performed using standard protocol. Antibodies used for detecting VEGFR2 signaling are listed in Key Resources Table. Quantification of WB signal was done by ImageJ software.

QUANTIFICATION AND STATISTICAL ANALYSIS

Results are expressed as the mean ± SEM. To calculate statistical significance, the two tailed Student's t-test (when comparing two groups) or one-way ANOVA followed by Tukey's multiple comparisons test (when comparing three or more groups) were used. Animal sample size was determined by power analysis (assuming 10% variability, 0.05 significance level, 90% power and SDev 8.5). *P value* <0.05 were considered significant. All calculations were performed using Prism software.

DATA AND SOFTWARE AVAILABILITY

The accession number for the RNA-seq and Chip-seq data reported in this paper is GSE94862 [Gene Expression Omnibus].